UNIVERSIDADE FEDERAL DE MINAS GERAIS
Instituto de Ciências Exatas
Programa de Pós-graduação em Física

João Renato Vaz Pires

REAL TIME TOTAL 3D RECONSTRUCTION OF RED BLOOD CELLS

Belo Horizonte
2025

João Renato Vaz Pires

REAL TIME TOTAL 3D RECONSTRUCTION OF RED BLOOD CELLS

Dissertation presented to the Graduate Program in Physics of the Institute of Exact Sciences of the Universidade Federal de Minas Gerais as parcial requirement for obtaining a Master's degree in Science.

Supervisor: Prof. Ubirajara Agero Batista

Co-supervisor: Prof. Lívia Siman Gomes

Belo Horizonte

2025

Dados Internacionais de Catalogação na Publicação (CIP)

P667r Pires, João Renato Vaz.
Real time total 3D reconstruction of red blood cells / João Renato Vaz Pires. – 2025.
75 f. : il.

Orientador: Ubirajara Agero Batista.
Coorientadora: Livia Siman Gomes.
Dissertação (mestrado) – Universidade Federal de Minas Gerais, Departamento de Física.
Bibliografia: f. 62-64.

1. Microscopia de desfocalização. 2. Eritrócitos. I. Título. II. Batista, Ubirajara Agero. III. Gomes, Livia Siman. IV. Universidade Federal de Minas Gerais, Departamento de Física.

CDU – 537.533.35(043)

Ficha catalográfica elaborada por Romário Martins Ribeiro – CRB6 3595
Biblioteca Professor Manoel Lopes de Siqueira – Departamento de Física - UFMG

UNIVERSIDADE FEDERAL DE MINAS GERAIS

INSTITUTO DE CIÊNCIAS EXATAS

PROGRAMA DE PÓS-GRADUAÇÃO EM FÍSICA

FOLHA DE APROVAÇÃO

A presente dissertação, intitulada **"Real Time Total 3d Reconstruction Of Red Blood Cells "** de autoria de **JOÃO RENATO VAZ PIRES** submetida à Comissão Examinadora, abaixo-assinada, foi aprovada para obtenção do grau de **MESTRE EM FÍSICA, área de concentração Física,** em 17 de julho de 2025.

Belo Horizonte, 17 de julho de 2025.

Prof. Ubirajara Agero Batista
Orientador do estudante
Departamento de Física/UFMG

Profa. Lívia Siman Gomes
Coorientadora do estudante
Departamento de Física/UFMG

Prof. Oscar Nassif de Mesquita
Departamento de Física/UFMG

Prof. Leonardo Teixeira Neves
Departamento de Física/UFMG

Prof. Pietro Cicuta
University of Cambridge

Documento assinado eletronicamente por **Livia Siman Gomes**, **Coordenador(a)**, em 18/07/2025, às 13:16, conforme horário oficial de Brasília, com fundamento no art. 5º do Decreto nº 10.543, de 13 de novembro de 2020.

Documento assinado eletronicamente por **Ubirajara Agero Batista**, **Servidor(a)**, em 04/08/2025, às 13:43, conforme horário oficial de Brasília, com fundamento no art. 5º do Decreto nº 10.543, de 13 de novembro de 2020.

Documento assinado eletronicamente por **Leonardo Teixeira Neves**, **Professor do Magistério Superior**, em 04/08/2025, às 17:33, conforme horário oficial de Brasília, com fundamento no art. 5º do Decreto nº 10.543, de 13 de novembro de 2020.

Documento assinado eletronicamente por **Pietro Cicuta**, **Usuário Externo**, em 02/09/2025, às 16:50, conforme horário oficial de Brasília, com fundamento no art. 5º do Decreto nº 10.543, de 13 de novembro de 2020.

Documento assinado eletronicamente por **Oscar Nassif de Mesquita**, **Usuário Externo**, em

Acknowledgements

Agradeço à minha família, aos meus pais Renato e Arlete e às minhas irmãs Mariana e Letícia, pelo carinho e apoio para seguir meus sonhos.

Agradeço à minha namorada Luana pela companhia, apoio, amor e carinho durante esses anos que estamos juntos. Que venham muitos mais, te amo Lulu.

Agradeço aos meus amigos Gabriel, Victor, Thiago, Matheus, Lucas e tantos outros pelo apoio, conversas e risadas compartilhadas.

Agradeço aos meus amigos e colegas do Laboratório de Física de Sistemas Biológicos, sem vocês, essa jornada teria sido muito menos agradável.

Agradeço à minha co-orientadora Lívia Siman pelo tempo, paciência, disponibilidade e ideias. Sei que seu tempo é curto, mas nem por isso você deixou de estar disponível para me ajudar quando precisei, desde os tempos de iniciação científica no laboratório.

Agradeço ao meu orientador Ubirajara Agero pela mentoria, disponibilidade, conversas, cervejas e apoio desde os tempos de IC. Obrigado por me mostrar que fazer ciência pode ser uma coisa leve e séria ao mesmo tempo e pelas oportunidades de aprendizado que tive no laboratório.

Agradeço às agências financiadoras: Conselho Nacional de Pesquisa e Desenvolvimento (CNPq), Fundação de Apoio a Pesquisa de Minas Gerais (FAPEMIG), Fundação Coordenação de Aperfeiçoamento de Pessoal de Nível Superior (CAPES) e ao Instituo Nacional de Ciência de Tecnologia de Fluidos Complexos (INCT-FCx).

Abstract

Defocusing Microscopy (DM) is a quantitative phase contrast microscopy technique based on the propagation of the electrical field through the microscope, which is used to obtain morphological and biomechanical parameters of different cells. On this dissertation, a geometrical model of the surface of a red blood cell was used to make a proof of concept for the total 3D reconstruction using DM. Furthermore, a new model for the angular spectrum of a phase object was studied and compared with the one used in previous works. Finally, we were able to make a computational routine to achieve the total 3D reconstruction of red blood cells in mediums with different osmolalities. Using this new routine, the results were obtained in $0.4s$ with high accuracy, representing an improvement from previous results, and enabling the total 3D reconstruction in real time.

Key-words: Defocusing microscopy, 3D total reconstruction, Red blood cells, Real time.

Resumo

A Microscopia de Desfocalização (MD) é uma técnica de microscopia de contraste de fase quantitativa baseada na propagação do campo elétrico pelo microscópio, que é utilizada para obter parâmetros morfológicos e biomecânicos de diferentes células. Neste trabalho, foi utilizado um modelo geométrico para a superfície de uma hemácia a fim de realizar uma prova de conceito para a reconstrução 3D total utilizando-se da MD. Além disso, foi estudado um novo modelo para o espectro angular de um objeto de fase e comparado o contraste obtido anteriormente e o obtido atualmente. Por fim, uma rotina computacional foi desenvolvida para a reconstrução 3D total de hemácias em meios com diferentes osmolalidades. Utilizando o programa, resultados são obtidos em cerca de $0.04s$ com alta acurácia, um avanço ao obtido anteriormente, e que viabiliza a reconstrução de células em tempo real.

Palavras-chave: Microscopia de Desfocalização, Reconstrução 3D de células, Hemácias, Tempo Real.

Contents

1 Introduction

Quantitative phase contrast microscopy is a powerful optical microscopy technique that seeks to non-invasively measure the morphology and dynamics of phase objects. One of the great advantages of using this type of microscopy is the ease of sample preparation when compared, for example, to fluorescence microscopy, and the increase in quantitative information obtained when compared to phase contrast microscopy methods, such as the discovery by Zernicke [1].

With quantitative phase contrast, the difference in refractive index between the analyzed object and the medium is used to create contrast in a previously transparent object, and can be divided into two groups: interference methods, which use interference between a reference laser and one that is scattered by the phase object [2] [3] [4] [5]; and non-interferometric methods, which reconstruct amplitude and phase information from the field scattered by a phase object in specific lighting situations [6] [7] [8].It is important to note that all phase contrast microscopy methods are, by nature, interferometric, since they are based on the interference of light directly transmitted through the sample with light scattered by it. The nomenclature used is simply to differentiate between techniques that actively use an interferometer and those that do not. Currently, there is an effort to integrate artificial intelligence into quantitative phase contrast microscopy techniques in order to improve the results obtained and facilitate the experimental process for obtaining the desired parameters. [9]. Various quantitative phase contrast microscopy techniques, both interferometric and non-interferometric, can be found in the book *Quantitative Phase Imaging of Cells and Tissues* [10]. Defocusing microscopy is a quantitative phase contrast microscopy technique developed and used at the Biological Systems Physics Laboratory of the Physics Department at UFMG that can be used to measure both biomechanical parameters and the morphology of phase objects. This work focuses on the analysis of the morphology of red blood cells in media with different osmolalities (a measure of the concentration of ions present in 1 kg of solution, a quantity used for the concentration of biological samples). Red blood cells were chosen for the study because they are easy to obtain, being collected by students in the laboratory, and because they have a particular characteristic: the absence of organelles inside them, which makes their refractive index constant and already known in the literature. [11] [12]. Chapter 2 briefly demonstrates the theory behind the construction of contrast used in defocusing microscopy, as well as a new model for the angular spectrum of any phase object, which results in an improvement in the expression of contrast used previously. In addition, a model for the surface of a red blood cell is presented, which is used to test computational routines. Chapter 3 presents the methodology used in this work, from the preparation of media with different osmolalities

to the computational work for acquiring parameters from the collected microscopy images. Chapter 4 presents the results obtained, which are total three-dimensional reconstructions of red blood cells in hypotonic, isotonic, and hypertonic media. Chapter 5 presents the conclusions and perspectives of the work. Finally, Appendix A contains the computational routine written in the *python* language used to generate three-dimensional profiles of red blood cells and extract the parameters of mean radius, volume, sphericity and surface area. Appendix B contains a guide on how to obtain 3D reconstruction using the *imageJ* software, commonly used for image analysis in the scientific community.

2 Theoretical Background

2.1 Defocusing Microscopy

Defocusing Microscopy (DM) is a quantitative phase contrast technique that can be used to analyze biomechanical and geometric parameters of phase objects. In this chapter, we will calculate the contrast generated by a phase object, analyzing the effect of one surface and two surfaces. We will also introduce an improvement on the model for the angular spectrum of a phase object with two surfaces, generating a new expression for this contrast. In addition, we will show how to recover the surfaces that make up this phase object using the DM contrast on two different focal planes.

To formulate the contrast expressions, let's start with Maxwell's equations and a brief review Fourier optics, and propagate the electric field through the defocused microscope.

Maxwell's equations in media without free charges are:

$$\nabla \cdot \vec{E} = 0; \tag{2.1}$$

$$\nabla \cdot \vec{B} = 0; \tag{2.2}$$

$$\nabla \times \vec{E} = -\frac{\partial \vec{B}}{\partial t}; \tag{2.3}$$

$$\nabla \times \vec{B} = \mu\varepsilon\frac{\partial \vec{E}}{\partial t}. \tag{2.4}$$

To find the wave equation, we calculate the curl of the equation 2.3:

$$\nabla \times \left(\nabla \times \vec{E}\right) = -\frac{\partial \left(\nabla \times \vec{B}\right)}{\partial t}. \tag{2.5}$$

Using the identity $\nabla \times (\nabla \times \vec{A}) = \nabla(\nabla \cdot \vec{A}) - \nabla^2\vec{A}$ alongside the equations 2.1 e 2.4:

$$-\nabla^2\vec{E} = -\mu\varepsilon\frac{\partial^2 \vec{E}}{\partial t^2}. \tag{2.6}$$

We have then successfully derived the wave equation. Assuming that the solution is a monochromatic plane wave of the kind $\vec{E}(\vec{r}, t) = \vec{E}(\vec{r})e^{i\omega t}$ and substituting it on 2.6:

$$\nabla^2\vec{E}(\vec{r}) = \omega^2\mu\varepsilon\vec{E}(\vec{r}). \tag{2.7}$$

Using $v = 1/\sqrt{\mu\varepsilon}$, and $k = \omega/v$, we get the Helmholtz equation:

$$\nabla^2 \vec{E}(\vec{r}) + k^2 \vec{E}(\vec{r}) = 0. \tag{2.8}$$

In a linear, isotropic, and homogeneous medium, we can consider that the electric field is the same in all directions. With this, we can consider 2.8 as a group of three identical scalar equations, one for each direction in space. This approximation is called the Scalar Theory of Diffraction, and we will use it for the propagation of the electric field in the microscope, together with Fourier optics.

2.1.1 Fourier Optics

First, let's define the Fourier transform $\mathcal{F}$. It is a mathematical tool that allows us to break down functions into the different frequencies and amplitudes that make them up. Mathematically, the two-dimensional Fourier transform is given by:

$$\mathcal{F}\left[f(\vec{x})\right] = \tilde{f}(\vec{k}) = \int_{-\infty}^{\infty} f(\vec{x}) e^{-i\vec{k}\cdot\vec{x}} d^2\rho \tag{2.9}$$

and the inverse transform:

$$\mathcal{F}^{-1}\left[\tilde{f}(\vec{k})\right] = f(\vec{x}) = \frac{1}{(2\pi)^2} \int_{-\infty}^{\infty} \tilde{f}(\vec{k}) e^{i\vec{k}\cdot\vec{x}} d^2k. \tag{2.10}$$

Let's now define some important properties of the Fourier transform:

1. Linearity: $\mathcal{F}\left[\alpha f + \beta g\right] = \alpha\mathcal{F}[f] + \beta\mathcal{F}[g]$;
2. Similarity theorem : $\mathcal{F}\left[f(\alpha\rho)\right] = \frac{1}{|\alpha|^2}\tilde{f}\left(\frac{q}{\alpha}\right)$;
3. Translation theorem: $\mathcal{F}\left[f(\rho - \alpha)\right] = \tilde{f}(q)e^{-iq\alpha}$;
4. Rayleigh's theorem (or Parseval's theorem): $\int_{-\infty}^{\infty} |f(\rho)|^2 d^2r\rho = \int_{-\infty}^{\infty} |\tilde{f}(q)|^2 d^2q$;
5. Convolution theorem: $\mathcal{F}\left[g * f\right] = \mathcal{F}[g] \cdot \mathcal{F}[f]$;
6. Derivadas: $\mathcal{F}[\nabla f(\rho)] = (-iq)\mathcal{F}[f(\rho)]$;

It is also important to define the angular spectrum of the electric field, given by its Fourier transform:

$$A(\vec{q}, z) = \int E(\vec{\rho}, z) e^{-i\vec{q}\cdot\vec{\rho}} d^2\rho, \tag{2.11}$$

and also the field as the inverse Fourier transform of the angular spectrum:

$$E(\vec{\rho}, z) = \frac{1}{(2\pi)^2} \int A(\vec{q}, z) e^{i\vec{\rho}\cdot\vec{q}} d^2q, \tag{2.12}$$

with $\vec{\rho} = x\hat{i} + y\hat{j}$ in the real space, and $\vec{q} = q_x\hat{i} + q_y\hat{j}$ in Fourier space, the spatial components in the plane perpendicular to the one of light propagation. Now we can define the propagation of light through the various components of the microscope.

2.1.1.1 Free space propagation

To find the equation for the free propagation of the angular spectrum, we just need to solve the Helmholtz equation 2.8 using the definition of the electric field as the inverse transform of the angular spectrum, that is, using equation 2.12. That is:

$$\nabla^2 \left(\frac{1}{(2\pi)^2} \int A(\vec{q}, z)\, e^{i\vec{\rho}\cdot\vec{q}} d^2q \right) + k^2 \left(\frac{1}{(2\pi)^2} \int A(\vec{q}, z)\, e^{i\vec{\rho}\cdot\vec{q}} d^2q \right) = 0. \tag{2.13}$$

Calculating the second derivatives and reorganizing:

$$\frac{1}{4\pi^2} \int \left[\left(k^2 - q^2 + \frac{\partial^2}{\partial z^2} \right) A(\vec{q}, z) \right] e^{i\vec{\rho}\cdot\vec{q}} d^2q = 0. \tag{2.14}$$

The only way this expression can be null is if the integrand is null. Defining $k_z^2 = k^2 - q^2$, we have:

$$-k_z^2 A(\vec{q}, z) = \frac{\partial^2 A(\vec{q}, z)}{\partial z^2}, \tag{2.15}$$

which has the following solution:

$$A(\vec{q}, z) = A(\vec{q}, 0)\, e^{\pm ik_z z} = A(\vec{q}, 0)\, e^{\pm ikz\sqrt{1-\frac{q^2}{k^2}}}. \tag{2.16}$$

The sign of the exponential function dictates the direction of light propagation. In this work, we will adopt the positive sign for propagation in the direction of the microscope's optical axis. We can then see that, when propagating the angular spectrum, we are adding a phase proportional to the distance traveled from our initial angular spectrum position. Finally, considering that the angle of light propagation and the optical axis is small, that is, $q^2 << k^2$, we can make the approximation $\sqrt{1 - \frac{q^2}{k^2}} \approx 1 - \frac{q^2}{2k^2}$. Thus, we have the final expression for the propagation of the angular spectrum in free space:

$$A(\vec{q}, z) = A(\vec{q}, 0)\, e^{\pm ik_z z} = A(\vec{q}, 0)\, e^{\ ikz} e^{-i\frac{zq^2}{2k}}. \tag{2.17}$$

To find the electric field, we just need to calculate the Fourier transform:

$$E(\vec{\rho}, z) = \frac{k}{2\pi i z} e^{ikz} \int E(\vec{\rho'}, 0) e^{\frac{ik}{2z}(\vec{\rho}-\vec{\rho'})^2} d^2\rho'. \tag{2.18}$$

2.1.1.2 Propagation through a thin lens

A thin lens only performs a transformation on the field's phase. The electric field, immediately after a thin lens, is given by:

$$E_l(\vec{\rho}) = t_l(\vec{\rho}) E_0(\vec{\rho}), \tag{2.19}$$

where $t_l(\vec{\rho})$ is the transmissivity of the lens, and is equal to:

$$t_l(\vec{\rho}) = e^{i\phi(\vec{\rho})}, \tag{2.20}$$

where

$$\phi(\vec{\rho}) = k_0 n_m \Delta_0 + k_0 (n_l - n_m) \Delta(\vec{\rho}). \tag{2.21}$$

With n_m being the refractive index of the media, and n_l the refractive index of the lens. $\Delta(\vec{\rho})$ and Δ_0 can be defined by dividing the lens into three parts: one convex, one flat, and one concave, as illustrated in Figure 1. The thicknesses of these parts are:

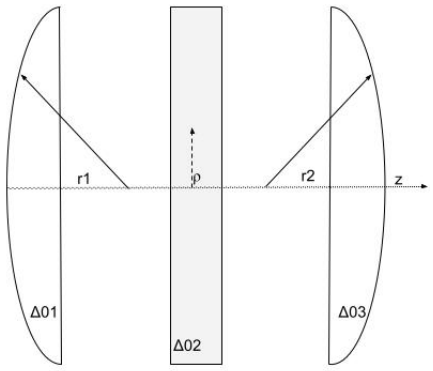

Figure 1 – Diagram of a lens.

$$\Delta_1(\vec{\rho}) = \Delta_{01} - r_1 \left(1 - \sqrt{1 - \frac{\rho^2}{r_1^2}}\right); \tag{2.22}$$

$$\Delta_2(\vec{\rho}) = \Delta_{02}; \tag{2.23}$$

$$\Delta_3(\vec{\rho}) = \Delta_{03} + r_2 \left(1 - \sqrt{1 - \frac{\rho^2}{r_2^2}}\right). \tag{2.24}$$

We can again make the paraxial approximation, as in the case of free propagation, $\sqrt{1-\frac{\rho^2}{R_i^2}} \approx 1 - \frac{\rho^2}{2R_i^2}$. Thus, we are left with:

$$\Delta(\vec{\rho}) = \Delta_0 - \frac{\rho^2}{2}\left(\frac{1}{r_1} - \frac{1}{r_2}\right). \tag{2.25}$$

Substituting 2.25 on 2.21, we obtain:

$$\phi(\vec{\rho}) = k_0 n_l \Delta_0 - k_0(n_l - n_m)\frac{\rho^2}{2}\left(\frac{1}{r_1} - \frac{1}{r_2}\right). \tag{2.26}$$

Using the Lensmaker's equation, given by:

$$\frac{1}{f} = \frac{n_l - n_m}{n_m}\left(\frac{1}{r_1} - \frac{1}{r_2}\right), \tag{2.27}$$

wwe can finally write our phase $\phi(\vec{\rho})$ as:

$$\phi(\vec{\rho}) = k_0 n_l \Delta_0 - \frac{k}{2f}\rho^2. \tag{2.28}$$

So, the electric field just after the lens, removing the terms that give us a constant phase change, is given by:

$$E_l(\vec{\rho}) = E_0(\vec{\rho})e^{-i\frac{k}{2f}\rho^2}. \tag{2.29}$$

To find the angular spectrum, we simply take the Fourier transform of 2.29:

$$A(\vec{q}, z) = \mathcal{F}\left[E_0(\vec{\rho})e^{-i\frac{k}{2f}\rho^2}\right]. \tag{2.30}$$

Using the convolution theorem, we get:

$$\begin{aligned} A(\vec{q}, z) &= \frac{1}{4\pi^2}\left\{\mathcal{F}\left[E_0(\vec{\rho}, z)\right] * \mathcal{F}\left[e^{-i\frac{k}{2f}\rho^2}\right]\right\} \\ A(\vec{q}, z) &= \frac{f}{2\pi i k}\int A_0(\vec{q'}, z)e^{i\frac{f}{2k}\left(\vec{q}-\vec{q'}\right)^2} d^2q'. \end{aligned} \tag{2.31}$$

With this, we are ready to propagate the electric field in the defocused microscope.

2.1.2 Electrical field propagation in the defocused microscope

Using equations 2.17, 2.31, and 2.29, we can propagate the electric field through the defocused microscope, as shown in image 2:

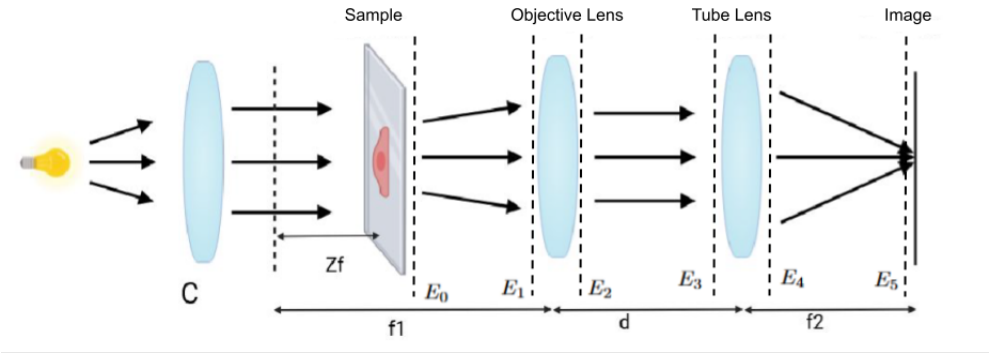

Figure 2 – Representation of the defocused microscope.

Let's divide the propagation into five parts:

1. Electric field E_0 from the sample propagates to the objective lens, becoming E_1;
2. Electric field E_1 passes through the objective lens, with focal length f_1, and becomes E_2;
3. Electric field E_2 just after the objective lens is propagated through free space to the tube lens, becoming E_3;
4. Field E_3 passes through the tube lens, with focal length f_2, becoming E_4;
5. Field E_4 propagates to the image plane, becoming E_5.

2.1.2.1 Field propagation to the objective lens

To propagate the field over a distance $f_1 - z_f$, we can use equation 2.18 to find the field E_1, and equation 2.17 to find its angular spectrum. We then have, for the electric field:

$$E_1(\vec{\rho}) = \frac{k}{2\pi i(f_1 - z_f)} e^{ik(f_1 - z_f)} \int E_0(\vec{\rho'}) e^{\frac{ik}{2(f_1 - z_f)}(\vec{\rho} - \vec{\rho'})^2} d^2\rho'. \tag{2.32}$$

And for the angular spectrum:

$$A_1(\vec{q}) = A_0(\vec{q}) e^{ik(f_1 - z_f)} e^{-i\frac{q^2(f_1 - z_f)}{2k}}. \tag{2.33}$$

2.1.2.2 Electric field after the objective lens

Now, we use equation 2.29 to find the field after the objective lens:

$$E_2(\vec{\rho}) = E_1(\vec{\rho}) e^{\frac{-ik}{2f_1}\rho^2}. \tag{2.34}$$

And the equation 2.31 to find its angular spectrum:

$$A_2(\vec{q}) = \frac{f_1}{2\pi i k} \int A_1(\vec{q'}) e^{\frac{if_1}{2k}(\vec{q}-\vec{q'})^2} d^2q'. \tag{2.35}$$

2.1.2.3 Propagation of the electric field to the tube lens

Again, we propagate the field through free space, now for a distance d using equation 2.18:

$$E_3(\vec{\rho}) = \frac{k}{2\pi i d} e^{ik_0 d} \int E_2(\vec{\rho'}) e^{\frac{ik_0}{2d}(\vec{\rho}-\vec{\rho'})^2} d^2\rho'. \tag{2.36}$$

and the angular spectrum using equation 2.17:

$$A_3(\vec{q}) = A_2(\vec{q}) e^{ik_0 d} e^{\frac{-iq^2 d}{2k_0}}. \tag{2.37}$$

2.1.2.4 Electric field after the tube lens

Now, we use equation 2.29 to find the field after the microscope's tube lens:

$$E_4(\vec{\rho}) = E_3(\vec{\rho}) e^{\frac{-ik_0}{2f_2}\rho^2}. \tag{2.38}$$

And, using equation 2.31, we obtain the angular spectrum:

$$A_4(\vec{q}) = \frac{f_2}{2\pi i k_0} \int A_3(\vec{q'}) e^{\frac{if_2}{2k_0}(\vec{q}-\vec{q'})^2} d^2q'. \tag{2.39}$$

2.1.2.5 Final electrical field

Finally, we need to propagate the field by a distance f_2 to the detector, where the image is formed. To do this, we use equation 2.18:

$$E_5(\vec{\rho}) = \frac{k_0}{2\pi i f_2} e^{ik_0 f_2} \int E_4(\vec{\rho'}) e^{\frac{ik_0}{2f_2}(\vec{\rho}-\vec{\rho'})} d^2\rho'. \tag{2.40}$$

And using equation 2.17, we also obtain the final angular spectrum:

$$A_5(\vec{q}) = A_4(\vec{q}) e^{ik_0 f_2} e^{-i\frac{q^2 f_2}{2k_0}}. \tag{2.41}$$

We now need to relate our final field E_5 to our initial field E_0, or our initial angular spectrum A_0. To do this, we start by substituting E_4 into E_5, and continue successively until we obtain our initial expression. The process is described in more detail in the appendix of [13]. We are left with:

$$E_5(\vec{\rho}) = J \int A_0\left(\vec{\rho'}\right) e^{i\frac{z_f}{2k}\rho'^2} e^{-\frac{if_1k_0}{f_2k}\vec{\rho}\cdot\vec{\rho'}} d^2\rho', \tag{2.42}$$

where J is:

$$J(\vec{\rho}) = \frac{-k_0 f_1}{4kf_2\pi^2} e^{i\left[k_0(f_2+d)+k(f_1-z_f)\right]} e^{i\frac{k_0}{2f_2}\left(1-\frac{d}{f_2}+\frac{f_1k_0}{f_2k}\right)\rho^2}. \tag{2.43}$$

We can see that when the focal plane is at the center of the phase object, i.e., $z_f = 0$, the electric field has the form:

$$E_5(\vec{\rho}) = J \int A_0(\vec{\rho'}) e^{-i\frac{f_1k_0}{f_2k}\vec{\rho}\cdot\vec{\rho'}} d^2\rho' = E_0\left(-\frac{f_1k_0}{f_2k}\vec{\rho}\right), \tag{2.44}$$

which is just the original electric field with a change of scale. We then see that, as expected, the phase object only adds a phase to the electric field, not changing the intensity measured in the microscope, unless the sample is defocused.

2.1.3 Angular spectrum of a phase object

2.1.3.1 Phase object with one interface

First, let us consider a flat phase object with a single interface, as shown in Figure 3.

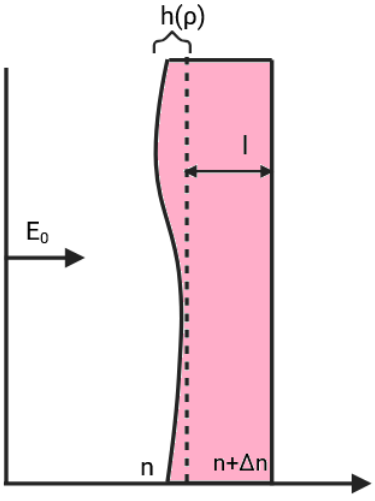

Figure 3 – Phase object with a single interface.

Considering the phase object to be approximately flat, we can say that its thickness is given by its average width l in addition to a small variation $h(\vec{\rho})$. We can also say that the refractive index of the phase object is close to that of the medium n_m, being $n_c = n_m + \Delta n$. Therefore, considering only the terms that depend on position, the phase that light gains when passing through this type of object is

$$\phi(\vec{\rho}) = n_m k_0 h(\vec{\rho}) - (n_m + \Delta n)\, k_0 h(\vec{\rho}) = \Delta n k_0 h(\vec{\rho}). \tag{2.45}$$

Assuming that the light arriving at the sample is a monochromatic plane wave, the electric field immediately after the sample is:

$$E(\vec{\rho}) = E_0 e^{i\phi(\vec{\rho})} = E_0 e^{i\Delta n k_0 h(\vec{\rho})}. \tag{2.46}$$

Considering again that $h(\vec{\rho})$ is small, we can write the electric field as:

$$E(\vec{\rho}) = E_0 \left(cos(\Delta n k_0 h(\vec{\rho}) + isen(\Delta n k_0 h(\vec{\rho})) \approx E_0 \left(1 + i\Delta n k_0 h(\vec{\rho})\right). \right. \tag{2.47}$$

To find the initial angular spectrum, we just need to take the Fourier transform of 2.47:

$$A_0(\vec{q}) = \mathcal{F}[E(\vec{\rho})] = E_0 \left(4\pi^2 \delta(\vec{q}) + i\Delta n k_0 \mathcal{F}[h(\vec{\rho})](\vec{q})\right) \tag{2.48}$$

Substituting this angular spectrum into 2.42, we obtain:

$$E(\vec{\rho}) = J \int E_0 \left(4\pi^2 \delta(\vec{q}) + i\Delta n k_0 \hat{h}(\vec{\rho'})\right) e^{i\frac{z_f}{2k}\rho'^2} e^{-\frac{if_1 k_0}{f_2 k}\vec{\rho}\cdot\vec{\rho'}} d^2\rho'$$

$$E(\vec{\rho}) = J E_0 \left[4\pi^2 + i\Delta n k_0 \int \hat{h}(\vec{\rho'}) e^{i\frac{z_f \rho'^2}{2k}} e^{-\frac{if_1 k_0}{f_2 k}\vec{\rho}\cdot\vec{\rho'}} d^2\rho'\right]. \tag{2.49}$$

In the small defocus regime (z_f small), we can expand the first exponential of the integral in 2.49, resulting in:

$$E(\vec{\rho}) = J E_0 \left\{4\pi^2 + i\Delta n k_0 \left[\int \hat{h}(\vec{\rho'}) e^{-\frac{if_1 k_0}{f_2 k}\vec{\rho}\cdot\vec{\rho'}} d^2\rho' + \int \hat{h}(\vec{\rho'}) \frac{iz_f}{2k} \rho'^2 e^{-\frac{if_1 k_0}{f_2 k}\vec{\rho}\cdot\vec{\rho'}} d^2\rho'\right]\right\}. \tag{2.50}$$

Rewriting the first integral, we can easily identify it as an inverse Fourier transform for $\mathcal{F}[h(\rho)]$:

$$\int \tilde{h}(\vec{\rho'}) e^{-\frac{if_1 k_0}{f_2 k}\vec{\rho}\cdot\vec{\rho'}} d^2\rho' = \int \tilde{h}(\vec{\rho'}) e^{i\left(\frac{-f_1 k_0}{f_2 k}\right)\vec{\rho}\cdot\vec{\rho'}} d^2\rho' = (2\pi)^2 h\left(-\frac{f_1 k_0}{f_2 k}\vec{\rho}\right) \tag{2.51}$$

To solve the second integral we can use the derivative property 6 of the Fourier transform:

$$\int \hat{h}(\vec{\rho'}) \frac{iz_f}{2k} \rho'^2 e^{\frac{-if_1 k_0}{f_2 k}\vec{\rho}\cdot\vec{\rho'}} d^2\rho' = -\frac{iz_f}{2k}\left(\frac{f_2 k}{f_1 k_0}\right)^2 \nabla_\rho^2 \int \hat{h}(\vec{\rho'}) e^{\frac{-if_1 k_0}{f_2 k}\vec{\rho}\cdot\vec{\rho'}} d^2\rho' = -\frac{iz_f}{2k}\left(\frac{f_2 k}{f_1 k_0}\right)^2 \nabla_\rho^2 h\left(\frac{-f_1 k_0}{f_2 k}\vec{\rho}\right) \tag{2.52}$$

So, we have the following as our final field:

$$E(\vec{\rho}) = 4\pi^2 J E_0 \left[1 + i\Delta n k_0 h\left(\frac{-f_1 k_0}{f_2 k}\vec{\rho}\right) + \frac{\Delta n z_f k}{2k_0}\left(\frac{f_2}{f_1}\right)^2 \nabla^2 h\left(\frac{-f_1 k_0}{f_2 k}\vec{\rho}\right)\right]. \tag{2.53}$$

The intensity observed on the detector becomes:

$$I(\vec{\rho}) = |E(\vec{\rho})|^2 \simeq I_0\left[1 - z_F \frac{\Delta n}{n_0}\left(\frac{k f_2}{k_0 f_1}\right)^2 \nabla^2 h\left(\frac{-f_1 k_0}{f_2 k}\vec{\rho}\right)\right], \tag{2.54}$$

where n_0 is the reefractive index of the objective oil. We can define the contrast of an image by:

$$C(\vec{\rho}) = \frac{I - I_0}{I_0}. \tag{2.55}$$

So, for a phase object with an single interface:

$$C(\vec{\rho}) = -z_f \frac{\Delta n}{n_0}\left(\frac{k f_2}{k_0 f_1}\right)^2 \nabla^2 h\left(\frac{-f_1 k_0}{f_2 k}\vec{\rho}\right). \tag{2.56}$$

2.1.3.2 Phase object with two interfaces

First, let's calculate the angular spectrum of a phase object with two roughly flat interfaces, as shown in image 4.

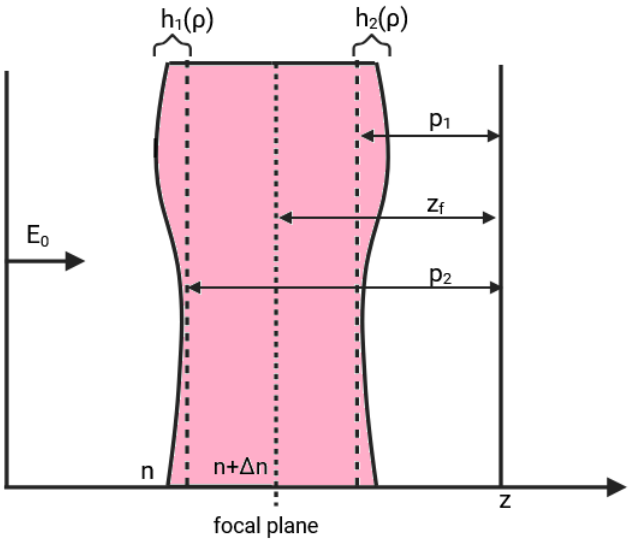

Figure 4 – Phase object with two interfaces.

To propagate the angular spectrum through the object with two interfaces, we will use three steps: Propagation through the first interface, gaining a phase $\Phi_1 = ik_0\Delta n h_1$; Propagation over a distance $p_2 - p_1$ between the interfaces; Propagation through the

second interface, gaining a phase $\Phi_2 = ik_0\Delta n h_2$. The field at each step is given by:

$$E_1(\vec{\rho}) = E_0 e^{i\Delta n k_0 h_1(\vec{\rho})}; \tag{2.57}$$

$$E_2(\vec{\rho}) = \frac{k e^{ik(p_1-p_2)}}{2\pi i(p_1-p_2)} \int E_1(\vec{\rho'}) e^{\frac{ik}{2(p_1-p_2)}(\vec{\rho}-\vec{\rho'})^2} d^2\rho'; \tag{2.58}$$

$$E_3(\vec{\rho}) = E_2(\vec{\rho}) e^{i\Delta n k_0 h_2(\vec{\rho})}. \tag{2.59}$$

Assuming the incident field as a monochromatic plane wave of constant amplitude, the field $E_3(\vec{\rho})$ will be:

$$E_3(\vec{\rho}) = E_0 \frac{k e^{ik(p_1-p_2)e^{i\Delta n k_0 h_2(\vec{\rho})}}}{2\pi i(p_1-p_2)} \int e^{i\Delta n k_0 h_1(\vec{\rho'})} e^{\frac{ik}{2(p_1-p_2)}(\vec{\rho'}-\vec{\rho})^2} d^2\rho'. \tag{2.60}$$

We can expand the exponentials containing $h_1(\vec{\rho'})$ and $h_2(\vec{\rho})$ in series and collect only the first terms, assuming that the interfaces are sufficiently thin. We are then left with:

$$E_3(\vec{\rho}) = E_0 \frac{k e^{ik(p_1-p_2)}}{2\pi i(p_1-p_2)} (1+i\Delta n k_0 h_2(\vec{\rho})) \left[-\frac{2\pi(p_2-p_1)}{ik} + i\Delta n k_0 \int h_1(\vec{\rho'}) e^{\frac{ik}{2(p_1-p_2)}(\vec{\rho'}-\vec{\rho})^2} d^2\rho' \right]. \tag{2.61}$$

Disregarding the term of order $h_1 h_2$, we obtain:

$$E_3(\vec{\rho}) = e^{ik(p_1-p_2)} \left[1 + i\Delta n k_0 h_2(\vec{\rho}) + \frac{i\Delta n k_0 k}{2\pi i(p_1-p_2)} \int h_1(\vec{\rho'}) e^{\frac{ik}{2(p_1-p_2)}(\vec{\rho'}-\vec{\rho})^2} d^2\rho' \right]. \tag{2.62}$$

Taking the Fourier transform, we can find the angular spectrum for a phase object with two interfaces:

$$A_3(\vec{q}) = E_0 e^{ik(p_1-p_2)} \left[4\pi^2\delta(\vec{q}) + i\Delta n k_0 \hat{h_2}(\vec{q}) + i\Delta n k_0 \hat{h_1}(\vec{q}) e^{\frac{-i(p_1-p_2)}{2k} q^2} \right]. \tag{2.63}$$

Performing the same procedure as in the previous subsection, we can obtain the contrast for an object with two flat interfaces:

$$C(\vec{\rho}) = (z_f - p_1)\frac{\Delta n}{n_0} \left(\frac{k f_2}{k_0 f_1} \right)^2 \nabla^2 h_1 \left(\frac{-k_0 f_1}{k f_2} \vec{\rho} \right) + (z_f - p_2)\frac{\Delta n}{n_0} \left(\frac{k f_2}{k_0 f_1} \right)^2 \nabla^2 h_2 \left(\frac{-k_0 f_1}{k f_2} \vec{\rho} \right). \tag{2.64}$$

In the case of a curved object, such as a red blood cell, we can simply replace the positions of membranes p_1 and p_2 with the functions $h_1(\vec{\rho})$ and $h_2(\vec{\rho})$, respectively, resulting in the coordinate system illustrated in Figure 5.

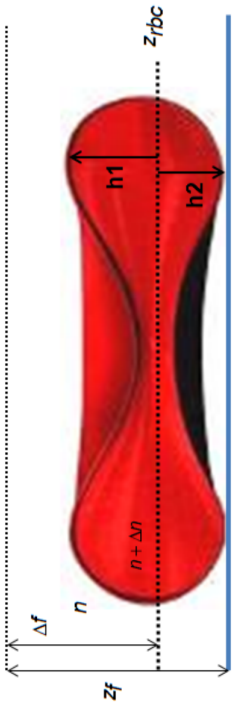

Figure 5 – Coordinate system used for a curved phase object. Taken from [13].

Doing this and omitting scale factors to condense the notation, we are left with:

$$C(\vec{\rho}) = \frac{\Delta n}{n_0}\left((\Delta f - h_1(\vec{\rho}))\nabla^2 h_1(\vec{\rho}) - (\Delta f - h_2(\vec{\rho}))\nabla^2 h_2(\vec{\rho})\right). \tag{2.65}$$

By changing the variables to the thickness $H(\rho) = h_1(\rho) - h_2(\rho)$ and asymmetry $\xi(\rho) = h_1(\rho) + h_2(\rho)$, we can rewrite the expression for the contrast as:

$$C(\rho) = \frac{\Delta n}{2n_0}\left(2\Delta f \nabla^2 H - H\nabla^2\xi - \xi\nabla^2 H\right). \tag{2.66}$$

To find the thickness $H(\rho)$, we must use two contrasts in different focal planes. Subtracting them, we obtain:

$$\Delta C = \frac{\Delta n}{n_0}(\Delta f_1 - \Delta f_2)\nabla^2 H, \tag{2.67}$$

which is a Poisson equation. Calculating the Fourier transform:

$$\mathcal{F}[\Delta C] = \frac{\Delta n}{n_0}(\Delta f_1 - \Delta f_2)q^2\mathcal{F}[H]. \tag{2.68}$$

Solving the equation for $H(\rho)$:

$$\begin{aligned}
\mathcal{F}\left[\Delta C\right] \frac{n_0}{\Delta n(\Delta f_1 - Delta f_2)} &= q^2 \mathcal{F}[H] \\
\mathcal{F}[H] &= \frac{\mathcal{F}\left[\Delta C\right]}{q^2} \frac{n_0}{\Delta n(\Delta f_1 - \Delta f_2)} \\
H &= \frac{n_0}{\Delta n(\Delta f_1 - \Delta f_2)} \mathcal{F}^{-1}\left[\frac{\mathcal{F}\left[\Delta C\right]}{q^2}\right].
\end{aligned} \tag{2.69}$$

To find the asymmetry ξ, we can use a contrast obtained in the focal plane, that is, $\Delta f = 0$. We are left with the following expression;

$$C(\rho) = -\frac{\Delta n}{2n_0}\left(H\nabla^2\xi + \xi\nabla^2 H\right). \tag{2.70}$$

Reorganizing:

$$\nabla^2\xi + \frac{\nabla^2 H}{H}\xi = -\frac{2Cn_0}{\Delta n}. \tag{2.71}$$

The equation has the form of a non-homogeneous Helmholtz equation with variable coefficients, and there is no general analytical solution for it. It is a type of equation found in seismology papers [14], and has an approximate analytical solution only in specific cases, with the coefficient of ξ varying slowly [15], which cannot be guaranteed in our context. The equation is solved numerically using the finite element method in this work. As we will see below, there is a wide variation of solutions with small changes in the boundary condition, which makes it difficult to process a large number of images. To solve this problem, a new contrast expression was developed from a better angular spectrum model for a phase object, presented in the next subsection.

2.1.4 Refinement of the model for the angular spectrum of a phase object

Another model for the angular spectrum of the electric field scattered by a phase object can be found from the Helmholtz equation, and is discussed in detail in [16]. We will derive it and use it to find a new contrast expression for defocusing microscopy.

The Helmholtz equation in a medium with a scattering object is given by:

$$\nabla^2 E(\vec{r}) + +k^2 n(\vec{r}) E(\vec{r}) = 0. \tag{2.72}$$

We can rewrite equation 2.72 in a more convenient way:

$$\nabla^2 E(\vec{r}) + k^2 E(\vec{r}) = -4\pi F(\vec{r}) E(\vec{r}), \tag{2.73}$$

where $F(\vec{r}) = k^2[n^2(\vec{r}) - 1]/k^2$ is called the scattering potential of the medium. Assuming that the total electric field is given by the sum of the incident field and the scattered field, i.e., $E = E_i + E_s$, and that the incident field obeys the traditional Helmholtz equation, we have:

$$(\nabla^2 + k^2)E_s(\vec{r}) = -4\pi F(\vec{r})E(\vec{r}). \tag{2.74}$$

We can transform this equation into an integral equation using Green's functions. We have:

$$(\nabla^2 + k^2)G(\vec{r} - \vec{r'}) = -4\pi\delta^{(3)}(\vec{r} - \vec{r'}). \tag{2.75}$$

Multiplying equation 2.74 by $G(\vec{r} - \vec{r'})$, equation 2.75 by $E_s(\vec{r})$ and subtracting 2.74 from 2.75 . We are left with:

$$E_s(\vec{r})\nabla^2 G(\vec{r}-\vec{r'}) - G(\vec{r}-\vec{r'})\nabla^2 E_s(\vec{r}) = 4\pi F(\vec{r})E(\vec{r})G(\vec{r}-\vec{r'}) - 4\pi E_s(\vec{r})\delta^{(3)}(\vec{r}-\vec{r'}). \tag{2.76}$$

Now we can integrate both sides of 2.76 into the variable r' in a volume V_R, bounded by a sphere of surface area S_R with radius R, which contains the scattering object inside, as shown on figure 6:

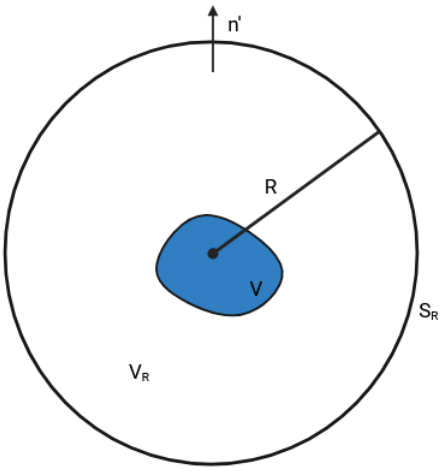

Figure 6 – Scatering object with volume V delimited by a sphere with radius R. The sphere has volume V_R and surface area S_R. The vector n' is normal to the sphere.

Using Green's theorem, we can convert the integral on the left side of 2.76 into a surface integral, and after a simple manipulation, we obtain:

$$E_s(\vec{r}) = \int_V F(\vec{r'})E(\vec{r'})G(\vec{r} - \vec{r'})d^3r' - \frac{1}{4\pi}\int_{S_R} E_s(\vec{r'})\frac{\partial G(\vec{r} - \vec{r'})}{\partial n'} - G(\vec{r} - \vec{r'})\frac{\partial E_s(\vec{r})}{\partial n'}dS_R. \tag{2.77}$$

We can make $R \to \infty$, so that it is reasonable to assume that the second integral on the right-hand side of 2.77 does not contribute to the scattered field. The chosen Green's function will be:

$$G(\vec{r} - \vec{r'}) = \frac{e^{ik|\vec{r}-\vec{r'}|}}{|\vec{r} - \vec{r'}|}. \tag{2.78}$$

Assuming that the incident field, coming from a direction $\hat{s_0}$, is given by a plane wave, that is, $E_i = e^{ik\hat{s_0}\cdot\vec{r}}$, we are left with the following expression for the electric field:

$$E(\vec{r}) = e^{ik\hat{s_0}\cdot\vec{r}} + \int_V F(\vec{r'})E(\vec{r'})\frac{e^{ik|\vec{r}-\vec{r'}|}}{|\vec{r} - \vec{r'}|}d^3r'. \tag{2.79}$$

This is called the integral equation of potential scattering. We cannot solve this equation directly, given the presence of the field itself within the integral, so we must resort to some technique to perform an approximation. A valid method in these cases is the perturbative method. Using it in the first order, we have:

$$E(\vec{r}) \approx E^{(1)}(\vec{r}) = e^{ik\hat{s_0}\cdot\vec{r}} + \int_V F(\vec{r'})e^{ik\hat{s_0}\cdot\vec{r'}}\frac{e^{ik|\vec{r}-\vec{r'}|}}{|\vec{r} - \vec{r'}|}d^3r'. \tag{2.80}$$

The unit vector $\hat{s_0}$ gives us the direction of the wave incident on the object. This solution is called Born's first-order approximation, and is sufficient for our application. In cases where multiple scattering occurs, a second-order expansion is necessary. We can focus our analysis on the second term of 2.80, which represents the scattered field. As we saw earlier, we need the angular spectrum of the field scattered by the phase object to develop the contrast of defocusing microscopy. Let us first deduce the angular spectrum for any object, and then apply it to our specific case. We then have, for the scattered field:

$$E_S^{(1)}(\vec{r}) = \int F(\vec{r'})e^{ik\hat{s_0}\cdot\vec{r'}}\frac{e^{ik|\vec{r}-\vec{r'}|}}{|\vec{r} - \vec{r'}|}d^3r'. \tag{2.81}$$

From now on, the subscript (1) related to the first order in Born approximation of the scattered field will be omitted, since we will always be within this approximation. As shown by H. Weyl in [17], we can write the spherical wave within the integral as:

$$\frac{e^{ik|\vec{r}-\vec{r'}|}}{|\vec{r} - \vec{r'}|} = \frac{ik}{2\pi}\iint_{-\infty}^{\infty}\frac{1}{s_z}e^{ik\hat{s}\cdot(|\vec{r}-\vec{r'}|)}ds_xds_y, \tag{2.82}$$

in which the unit vector $\hat{s}$ gives the direction of the scattered wave and s_i is the i component of this vector. Substituting 2.82 in 2.81, we get:

$$E_S(\vec{r}) = \int_V F(\vec{r'})e^{ik\hat{s_0}\cdot\vec{r'}}\iint_{\infty}^{\infty}\frac{ik}{2\pi s_z}e^{ik[\hat{s}\cdot(\vec{r}-\vec{r'})]}ds_xds_yd^3r'. \tag{2.83}$$

We can reorganize the exponential terms of this integral in a more convenient way:

$$\begin{aligned} E_S(\vec{r}) &= \int_V d^3r' \iint_\infty^\infty ds_x ds_y \frac{ik}{2\pi s_z} F(\vec{r'}) e^{-ik[(\hat{s}-\hat{s_0})\cdot\vec{r'}]} e^{ik\hat{s}\cdot\vec{r}} \\ E_S(\vec{r}) &= \iint_\infty^\infty a(s_x, s_y) e^{ik\hat{s}\cdot\vec{r}} ds_x ds_y, \end{aligned} \tag{2.84}$$

in which $a(s_x, s_y)$ is a term proportional to the Fourier transform of $F(r')$, at frequency $k(s_i - s_{0i})$:

$$\begin{aligned} a(s_x, s_y) &= \int_V \frac{ik}{2\pi s_z} F(\vec{r'}) e^{-ik[(\hat{s}-\hat{s_0})\cdot\vec{r'}]} d^3r' \\ &= \frac{ik}{2\pi s_z} \tilde{F}[k(s_x - s_{0x}), k(s_y - s_{0y}), k(s_z - s_{0z})]. \end{aligned} \tag{2.85}$$

If we calculate the spatial Fourier transform in the x, y plane of 2.84, we obtain

$$A_s = \frac{(2\pi)^2}{k^2} a(s_x, s_y) e^{iks_z z}. \tag{2.86}$$

Reorganizing:

$$a(s_x, s_y) = \frac{k^2}{(2\pi)^2} A_s e^{-iks_z z}. \tag{2.87}$$

We then obtain two expressions for the term $a(s_x, s_y)$. Equating 2.85 and 2.87:

$$\frac{ik}{2\pi s_z} \tilde{F} = \frac{k^2}{(2\pi)^2} A_s e^{-iks_z Z}. \tag{2.88}$$

We then have, as a general expression for the angular spectrum of the field scattered by an object:

$$A_S = \frac{2\pi i}{k s_z} e^{-iks_z Z} \int F(\vec{r}) e^{-ik[(s_x - s_{0x})x' + (s_y - s_{0y})y' + (s_z - s_{0z})z']} d^3r'. \tag{2.89}$$

With the general expression derived, we can derive the expression for a phase object with two surfaces, as shown on figure 7.

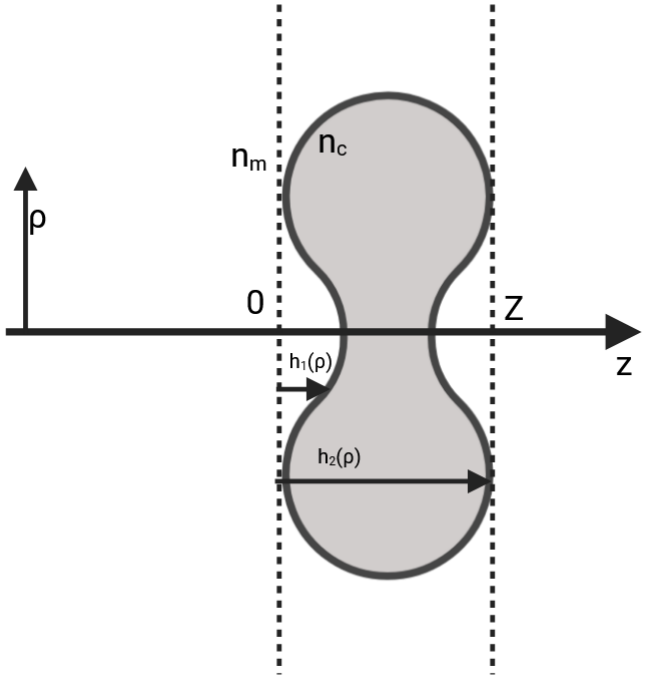

Figure 7 – Phase object located between 0 and Z. The surfaces $h_1(\rho)$ and $h_2(\rho)$ are the lower and upper membrane of the phase object. The media refraction index is now denoted as n_m and the phase object's n_c.

We can assume that the wave strikes the phase object only in the z direction, so $s_{0x} = s_{0y} = 0$. We will also change the notation to match the one used to find the expression for the electric field in the image plane found earlier. That is, $ks_x + ks_y = q$ and $x' + y' = \rho'$. Substituting the expression for the scattering potential, we get:

$$A_s = \frac{2\pi i}{k_z} e^{-ik_z Z} \int \frac{k_0}{4\pi} [n^2(r') - n_m^2] e^{-iq\rho'} e^{-i(k_z - k_{0z})z'} d\rho' dz', \tag{2.90}$$

where n_m is the refractive index of the medium in which our phase object is inserted. Looking at figure 7, we can see that the integral is non zero only in the regions between the surfaces $h_1(\rho)$ and $h_2(\rho)$, since outside of it $n(r') = n_m$, zeroing the term in parentheses. Being n_o the refractive index of the phase object, we have:

$$\begin{aligned} A_s &= \frac{2\pi i}{k_z} e^{ik_z Z} \int d^2\rho' \frac{k_0}{4\pi} (n_c^2 - n_m^2) e^{-iq\rho'} \int_{h_1(\rho')}^{h_2(\rho')} dz' e^{i(k_z - k_{0z})z'} \\ &= \frac{2\pi i}{k_z} e^{ik_z Z} \int d^2\rho' \frac{k_0}{4\pi} (n_c^2 - n_m^2) e^{-iq\rho'} \frac{e^{-i(k_z - k_{0z})h_2} - e^{-i(k_z - k_{0z})h_1}}{-i(k_z - k_{0z})} \\ A_S &= \frac{2\pi i}{k_z} e^{ik_z Z} \frac{k_0 (n_c^2 - n_m^2)}{4\pi} \int d^2\rho' e^{iq\rho'} \frac{e^{-i(k_z - k_{0z})h_2} - e^{-i(k_z - k_{0z})h_1}}{-i(k_z - k_{0z})}. \end{aligned} \tag{2.91}$$

Since we are working within the paraxial approximation, we have that $k_z = \sqrt{k_0^2 - q^2} \approx$

$k_0(1 - q^2/2k_0^2)$. Thus, we can rewrite 2.91:

$$A_s = \frac{2\pi i}{k_z} e^{ik_0 Z} e^{-i\frac{q^2 z}{2k_0}} \frac{k_0(n_c^s - n_m^2)}{4\pi} \int d^2\rho' e^{-iq\rho'} \frac{2k_0}{iq^2} \left[e^{\frac{iq^2}{2k_0}h_2} - e^{\frac{iq^2}{2k_0}h_1} \right]. \tag{2.92}$$

We now have the final equation for the angular spectrum of a phase object with two interfaces. All that remains is to substitute it into equation 2.92 to find a new contrast equation for an out-of-focus object. Recalling the final electric field of the defocused microscope:

$$E(\vec{\rho}) = \int A_0 e^{\frac{iz_f q^2}{2k}} e^{-i\frac{f_1}{f_2}\frac{k_0}{k}\rho q} d^2q. \tag{2.93}$$

Making the change $n_m k_0 = k_m$ and substituting the equation found for the scattered angular spectrum:

$$E(\vec{\rho}) = \int d^2q \int d^2\rho' \frac{2\pi i}{k_m} e^{ik_m Z} e^{-i\frac{q^2 Z}{2k_m}} \frac{k_0[n_c^2 - n_m^2]}{4\pi} e^{-iq\rho'} \frac{2k_0}{iq^2} \left[e^{\frac{iq^2}{2k_0}h_2} - e^{\frac{iq^2}{2k_0}h_1} \right] e^{\frac{iz_f q^2}{2k}} e^{-i\frac{f_1}{f_2}\frac{k_0}{k}\rho q}. \tag{2.94}$$

Reorganizing the terms and replacing the term k_z in the denominator of the first fraction with k_m, since before the scattering $k_z = k_m$:

$$E(\vec{\rho}) = \frac{2\pi i}{k_m} e^{ik_m Z} e^{i\frac{q^2}{2k_m}(\frac{n_m}{n_0}z_f - Z)} \frac{k_0^2[n_c^2 - n_m^2]}{4\pi} \frac{2k_m}{iq^2} \int d^2q e^{i\rho q} \int d^2\rho' e^{-iq\rho'} \left[e^{\frac{iq^2}{2k_m}h_2} - e^{\frac{iq^2}{2k_m}h_1} \right]. \tag{2.95}$$

Grouping the terms with q^2 in the exponent and simplifying:

$$E(\vec{\rho}) = \frac{ik_0}{2} e^{ik_m Z} \frac{[n_c^2 - n_m^2]}{n_m} \frac{2k_m}{iq^2} \int d^2q e^{i\rho q} \int d^2\rho' \left[e^{\frac{iq^2}{2k_m}\left(h_2 + \frac{n_m}{n_0}z_f - Z\right)} - e^{\frac{iq^2}{2k_m}\left(h_1 + \frac{n_m}{n_0}z_f - Z\right)} \right], \tag{2.96}$$

where n_0 is the refractive index of the objective oil. Now, we can move our origin to the other end of our phase object, as shown in Figure 8.

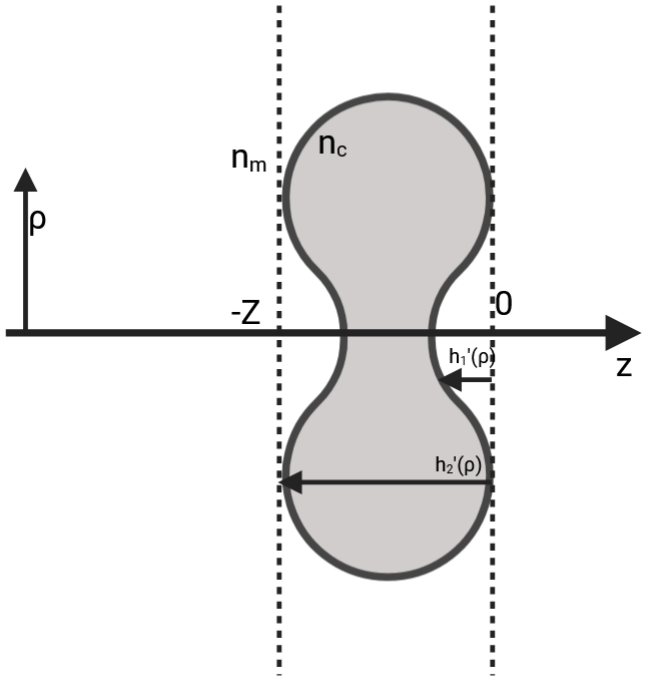

Figure 8 – Phase object with coordinate change.

Performing the change in equation 2.96:

$$E_{(}\vec{\rho}) = \frac{ik_0}{2} e^{ik_m Z} \frac{[n_c^2 - n_m^2]}{n_m} \frac{2k_m}{iq^2} \int d^2q e^{iq\rho} \int d^2\rho' e^{-iq\rho'} \left[e^{\frac{iq^2}{2k_m}\left(-h_1' + \frac{n_m}{n_0} z_f\right)} - e^{\frac{iq^2}{2k_m}\left(h_2' + \frac{n_m}{n_0} z_f\right)} \right]. \tag{2.97}$$

We then have a new expression for the final scattered field of defocusing microscopy. To construct the contrast, we need the intensity. Since $E = E_i + E_s$, we have:

$$I = |E_i|^2 + E_i^* E_s + E_s^* E_i + |E_s|^2. \tag{2.98}$$

Within Born's first approximation, we can disregard the term $|E_s|^2$. We have for contrast:

$$C = \frac{I - I_0}{I_0} = \frac{|E_i|^2 + E_i^* E_s + E_s^* E_i - |E_i|^2}{|E_i|^2} = \frac{E_s}{E_i} + \frac{E_s^*}{E_i^*}. \tag{2.99}$$

Opening the complex fields in their real and imaginary parts, we get:

$$C = 2\mathcal{R}e\left\{\frac{E_s}{E_i}\right\}. \tag{2.100}$$

Making the incident field as $E_i = e^{ik_m Z}/(2\pi)^2$, and making the changes $h_2' \to h_2$, $h_1' \to h_1$ for notation purposes:

$$\frac{E_s}{E_i} = \frac{1}{(2\pi)^2}\frac{k_0 k_m}{q^2}\frac{[n_c^2 - n_m^2]}{n_m}\int d^2q e^{iq\rho}\int d^2\rho' e^{-iq\rho'}\left[e^{\frac{iq^2}{2k_m}\left(-h_1+\frac{n_m}{n_0}z_f\right)} - e^{\frac{iq^2}{2k_m}\left(h_2+\frac{n_m}{n_0}z_f\right)}\right]. \tag{2.101}$$

In the regime of thin objects and small defocusing, we can expand the exponentials of 2.101 in Taylor series:

$$e^{\frac{iq^2}{2k_m}\left(-h_1+\frac{n_m}{n_0}z_f\right)} \approx \frac{iq^2}{2k_m}\left(-h_1+\frac{n_m}{n_0}z_f\right) - \frac{q^4}{8k_m^2}\left(-h_1+\frac{n_m}{n_0}z_f\right)^2 + \mathcal{O}^3; \tag{2.102}$$

$$e^{\frac{iq^2}{2k_m}\left(h_2+\frac{n_m}{n_0}z_f\right)} \approx \frac{iq^2}{2k_m}\left(-h_2+\frac{n_m}{n_0}z_f\right) - \frac{q^4}{8k_m^2}\left(-h_2+\frac{n_m}{n_0}z_f\right)^2 + \mathcal{O}^3. \tag{2.103}$$

Since we only want the real part, we will collect only the second term of each expansion. Substituting in 2.101:

$$\begin{aligned}\frac{E_s}{E_i} &= \frac{1}{(2\pi)^2}\frac{k_0 k_m}{q^2}\frac{[n_c^2 - n_m^2]}{n_m}\int d^2q e^{iq\rho}\int d^2\rho' e^{-iq\rho'}\frac{-q^4}{8k_m^2}\left[\left(-h_1+\frac{n_m}{n_0}z_f\right)^2 - \left(-h_2+\frac{n_m}{n_0}z_f\right)^2\right] \\ &= \frac{1}{(2\pi)^2}\frac{[n_c^2 - n_m^2]}{n_m^2}\int d^2q e^{iq\rho}\int d^2\rho' e^{-iq\rho'}\frac{-q^2}{8}\left[\left(-h_1+\frac{n_m}{n_0}z_f\right)^2 - \left(-h_2+\frac{n_m}{n_0}z_f\right)^2\right].\end{aligned} \tag{2.104}$$

We can use the derivative property, given in equation 6, to make $q^2 \to \nabla^2$. Finally, we identify the integrals as a Fourier transform and an inverse Fourier transform. Thus:

$$\frac{E_s}{E_i} = -\frac{[n_c^2 - n_m^2]}{8n_m^2}\nabla^2\left[\left(-h_1+\frac{n_m}{n_0}z_f\right)^2 - \left(-h_2+\frac{n_m}{n_0}z_f\right)^2\right]. \tag{2.105}$$

Substituting it in the expression 2.100 found for the contrast:

$$C = \frac{[n_m^2 - n_c^2]}{4n_m^2}\nabla^2\left[\left(-h_1+\frac{n_m}{n_0}z_f\right)^2 - \left(-h_2+\frac{n_m}{n_0}z_f\right)^2\right]. \tag{2.106}$$

We can simplify this expression even further by expanding the notable products within the Laplacian operator:

$$\begin{aligned}C &= \frac{[n_m^2 - n_c^2]}{4n_m^2}\nabla^2\left[h_1^2 - \frac{2n_m}{n_0}h_1 z_f + \left(\frac{n_m}{n_0}z_f\right)^2 - \left(h_2^2 - \frac{2n_m}{n_0}h_2 z_f + \left(\frac{n_m}{n_0}z_f\right)^2\right)\right] \\ &= \frac{[n_m^2 - n_c^2]}{4n_m^2}\nabla^2\left[h_1^2 - h_2^2 - \frac{2n_m z_f}{n_0}(h_1 - h_2)\right] \\ &= \frac{[n_m^2 - n_c^2]}{4n_m^2}\nabla^2\left[(h_1 - h_2)(h_1 + h_2) - \frac{2n_m z_f}{n_0}(h_1 - h_2)\right].\end{aligned} \tag{2.107}$$

Making the variable changes again: $h_1 - h_2 = H$ and $h_1 + h_2 = \xi$:

$$C = \frac{[n_m^2 - n_c^2]}{4n_m^2}\nabla^2\left[H\xi + \frac{2n_m}{n_0}z_f H\right]. \tag{2.108}$$

This is our final equation for the contrast of a phase object. We can see, if we compare it with the expression 2.66, used previously, that we have a simpler expression, now in the form of a Poisson equation. This allows us to find the morphological parameters of phase objects more quickly and efficiently, making it possible to solve it analytically for thickness H and asymmetry ξ.

To find the variables H and ξ, and consequently the surfaces h_1 and h_2, we must first find the thickness H. To do this, we must capture two images at different focal planes, subtract the contrasts, and solve a Poisson equation. Mathematically:

$$C_1 - C_2 = \Delta C = \frac{[n_m^2 - n_c^2]}{4n_m^2}\nabla^2\left[\frac{2n_m}{n_0}(z_{f1} - z_{f2})H\right]$$

$$\frac{2n_m}{n_0}\Delta z_f \nabla^2 H = \frac{4n_m^2\Delta C}{[n_m^2 - n_c^2]}$$

$$\nabla^2 H = \frac{2\Delta C n_0 n_m}{[n_c^2 - n_m^2]\Delta z_f}$$

$$\mathcal{F}[H] = \frac{2n_0 n_m}{[n_c^2 - n_m^2]\Delta z_f}\mathcal{F}[\Delta C]$$

$$q^2\mathcal{F}[H] = \frac{2n_0 n_m}{[n_c^2 - n_m^2]\Delta z_f}\mathcal{F}\left[\Delta C\right]$$

$$\mathcal{F}[H] = \frac{2n_0 n_m}{[n_c^2 - n_m^2]\Delta z_f}\frac{\mathcal{F}\left[\Delta C\right]}{q^2}$$

$$H = \frac{2n_0 n_m}{[n_c^2 - n_m^2]\Delta z_f}\mathcal{F}^{-1}\left[\frac{\mathcal{F}\left[\Delta C\right]}{q^2}\right]. \tag{2.109}$$

In posession of H, we can find the asymmetry ξ. Taking an image on any focal plane where the objects contrast is linear, we can find ξ as follows:

$$C = \frac{[n_m^2 - n_c^2]}{4n_m^2}\nabla^2\left[H\xi + \frac{2n_m}{n_0}z_f H\right]$$

$$\frac{4n_m^2}{[n_m^2 - n_c^2]}C = \nabla^2\left[H\xi + \frac{2n_m}{n_0}z_f H\right]$$

$$\frac{4n_m^2}{[n_m^2 - n_c^2]}\mathcal{F}[C] = q^2\left[\mathcal{F}\left[H\xi\right] + \frac{2n_m}{n_0}z_f\mathcal{F}[H]\right]$$

$$\frac{4n_m^2}{[n_m^2 - n_c^2]}\frac{\mathcal{F}[C]}{q^2} = \mathcal{F}\left[H\xi\right] + \frac{2n_m}{n_0}z_f\mathcal{H}$$

$$\mathcal{F}\left[H\xi\right] = \frac{4n_m^2}{[n_m^2 - n_c^2]}\frac{\mathcal{F}[C]}{q^2} - \frac{2n_m}{n_0}z_f\mathcal{F}[H]$$
$$H\xi = \frac{4n_m^2}{[n_m^2 - n_c^2]}\mathcal{F}^{-1}\left[\frac{\mathcal{F}[C]}{q^2}\right] - \frac{2n_m}{n_0}z_f H$$
$$\xi = \frac{4n_m^2}{H[n_m^2 - n_c^2]}\mathcal{F}^{-1}\left[\frac{\mathcal{F}[C]}{q^2}\right] - \frac{2n_m}{n_0}z_f. \tag{2.110}$$

Thus, by solving two Poisson equations, we obtain the surfaces of both membranes of a phase object using only two images obtained at different focal planes. The membranes are given by:

$$h_1(\rho) = \frac{\xi + H}{2} = \frac{2n_m^2}{H[n_m^2 - n_c^2]}\mathcal{F}^{-1}\left[\frac{\mathcal{F}[C]}{q^2}\right] - \frac{n_m}{n_0}z_f + \frac{n_0 n_m}{[n_c^2 - n_m^2]\Delta z_f}\mathcal{F}^{-1}\left[\frac{\mathcal{F}\left[\Delta C\right]}{q^2}\right] \tag{2.111}$$

$$h_2(\rho) = \frac{\xi - H}{2} = \frac{2n_m^2}{H[n_m^2 - n_c^2]}\mathcal{F}^{-1}\left[\frac{\mathcal{F}[C]}{q^2}\right] - \frac{n_m}{n_0}z_f - \frac{n_0 n_m}{[n_c^2 - n_m^2]\Delta z_f}\mathcal{F}^{-1}\left[\frac{\mathcal{F}\left[\Delta C\right]}{q^2}\right]. \tag{2.112}$$

It is important to note another difference between the new and traditional equations: previously, we made the approximation $z_f \approx \Delta f$, such as in [18] [19], and considered the minimum contrast plane at the center of the red blood cell with $\Delta f = 0$. In this work, we do not make this approximation, and as shown in Figure 5, z_f is the distance from the coverslip to the focal plane. The exact position of the lamella in the z-axis is extremely difficult to locate experimentally, requiring the preparation of a lamella with polystyrene microspheres, and that the microspheres be close to the sample at the time of image capture, but far enough away so that there is no physical contact and the light scattered by the sphere does not interfere with that scattered by the red blood cell.

Given this difficulty, as the term containing z_f is only a constant that is subtracted from the expression for each membrane, it only translates our total 3D reconstruction vertically, without interfering with the obtention of any of the parameters that are of interest for analysis. The experiments for the validation of the new equation were performed with coverslips without polystyrene microspheres.

2.2 Geometric representation of the surface of a red blood cell

As a way to theoretically validate the use of defocusing microscopy to obtain geometric reconstruction of cells, we use the geometric representation of red blood cells, already well known and first demonstrated by Kuchel in [20] and explored in [21]. The equation that better approximates the shape of a red blood cell is the one of a degree-4 surface, such as:

$$\left(x^2 + y^2 + z^2\right)^2 + P\left(x^2 + y^2\right) + Qz^2 + R = 0, \tag{2.113}$$

in which the coefficients P, Q, and R are adjusted according to the geometric characteristics of the red blood cell to be generated. To find the explicit forms of these parameters, it is convenient to rewrite equation 2.113 in cylindrical coordinates:

$$\left(\rho^2 + z^2\right)^2 + P\rho^2 + Qz^2 + R = 0. \tag{2.114}$$

The required red blood cell parameters are its diameter d, its maximum height h, and its height at the center b, as shown on image 9.

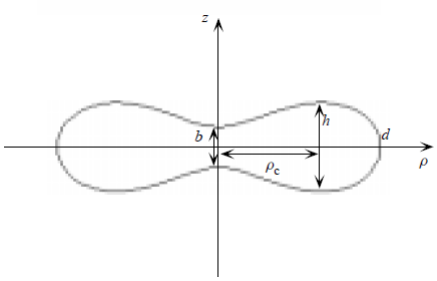

Figure 9 – Red blood cell surface parameters. [20]

We can obtain three equations to determine P, Q and R as a function of b, d and h, analyzing 3 points of interest in 9:

1. At the center ($\rho = 0$ and $z = b/2$):

$$\frac{b^4}{16} + Q\frac{b^2}{4} + R = 0 \tag{2.115}$$

2. At the edges ($\rho = d/2$ e $z = 0$):

$$\frac{d^4}{16} + P\frac{d^2}{4} + R = 0 \tag{2.116}$$

3. At the maximum height point ($\rho = \rho_c$ e $z = h/2$):

$$P^2 + h^2(P - Q) - 4R = 0 \tag{2.117}$$

If we solve 2.115 and 2.116 together, we obtain an equation for Q as a function of P:

$$Q = P\frac{d^2}{b^2} + \frac{b^2}{4}\left(\frac{d^4}{b^4} - 1\right). \tag{2.118}$$

Using equation 2.116, we also arrive at an expression for R as a function of P:

$$R = \frac{-d^2}{4}\left(P + \frac{d^2}{4}\right). \tag{2.119}$$

Substituting 2.118 and 2.119 into 2.117, we finally obtain an equation for P:

$$P^2 + h^2 P - h^2\left[P\frac{d^2}{b^2} + \frac{b^2}{4}\left(\frac{d^4}{b^4} - 1\right)\right] + d^2\left(P - \frac{d^2}{4}\right)$$

$$P^2 + P\left[d^2 - h^2\left(\frac{d^2}{b^2} - 1\right)\right] + \left[\frac{d^4}{4} - \frac{h^2 b^2}{4}\left(\frac{d^4}{b^4} - 1\right)\right] = 0. \tag{2.120}$$

Equation 2.120 is a quadratic equation, so it has two solutions, denoted P_+ and P_-:

$$P_+ = -\frac{d^2}{2} + \frac{h^2}{2}\left(\frac{d^2}{b^2} - 1\right) - \frac{h^2}{2}\left(\frac{d^2}{b^2}\right)\sqrt{1 - \frac{b^2}{h^2}}; \tag{2.121}$$

$$P_- = -\frac{d^2}{2} + \frac{h^2}{2}\left(\frac{d^2}{b^2} - 1\right) + \frac{h^2}{2}\left(\frac{d^2}{b^2}\right)\sqrt{1 - \frac{b^2}{h^2}}. \tag{2.122}$$

We then need to find which of the solutions for P gives us a value that is consistent with the surface of a red blood cell. To do this, we can derive the expression 2.114 in ρ. Doing so, we obtain:

$$4\rho\left(\rho^2 + z^2\right) + 4z\frac{dz}{d\rho}\left(\rho^2 + z^2\right) + 2P\rho + 2Qz\frac{dz}{d\rho} = 0$$

$$2\left(\rho^2 + z^2\right)\left(\rho + z\frac{dz}{d\rho}\right) + P\rho + Qz\frac{dz}{d\rho} = 0. \tag{2.123}$$

Looking again at Figure 9, which represents a meridional cross section of the surface, we observe three points where $\frac{dz}{d\rho} = 0$: at the center of the red blood cell and at the two points where $\rho = \rho_c$. To observe these points in the surface equation, we can set $\frac{dz}{d\rho} = 0$ in equation 2.123:

$$2\rho\left(\rho^2 + z^2\right) + P\rho = 0$$

$$\rho\left(\rho^2 + z^2 + \frac{P}{2}\right) = 0. \tag{2.124}$$

we see that $\rho = 0$ satisfies this equation. Substituting $\rho = \rho_c$, and setting $z = h/2$ to analyze the maximum points:

$$\rho_c^2 + \frac{h^2}{4} = -\frac{P}{2}$$

$$-\left(2\rho_c^2+\frac{h^2}{2}\right)=P. \tag{2.125}$$

So we see, then, that for equation 2.113 to represent a biconcave erythrocyte, the condition $P<0$ must necessarily be satisfied. We need to choose between P_+ and P_- the solution that presents $P<0$ for the usual parameters d, h and b of a red blood cell. This solution is P_+, since in the region of interest of $d>h>b$, as is the case for the vast majority of red blood cells, $P_+<0$ always.

2.2.1 Surface plot

To plot the surface, we first need to solve equation 2.114 for z. Expanding the term $(\rho^2+z^2)^2$ we get:

$$\rho^4+z^4+2\rho^2z^2+P\rho^2+Qz^2+R=0$$

$$z^4+\left(2\rho^2+Q\right)z^2+\left(\rho^4+P\rho^2+R\right)=0. \tag{2.126}$$

We can see that equation 2.126 is a biquadratic equation for z. Substituting $z^2=Z$, we are left with only one quadratic equation to solve:

$$Z^2+\left(2\rho^2+Q\right)Z+\left(\rho^4+P\rho^2+R\right)=0. \tag{2.127}$$

Solving it, we obtain the roots:

$$Z_+=\frac{-\left(2\rho^2+Q\right)+\sqrt{\Delta}}{2}; \tag{2.128}$$

$$Z_-=\frac{-\left(2\rho^2+Q\right)-\sqrt{\Delta}}{2}, \tag{2.129}$$

where Δ is:

$$\Delta=\left(2\rho^2+Q\right)^2-4\left(\rho^4+P\rho^2+R\right)$$

$$\Delta=4\rho^4+Q^2+4\rho^2Q-4\rho^4-4P\rho^2-4R$$

$$\Delta=Q^2+4\rho^2Q-4P\rho^4-4R. \tag{2.130}$$

Since $z=\pm\sqrt{Z}$, and necessarily, $z\in\mathbb{R}$ since it represents the surface, the solution of 2.127 that interests us is 2.128. We are left with solutions for both membranes, with z_+ denoting the upper membrane and z_- the lower one.

$$z_+ = \sqrt{Z_+} = \left[\frac{-\left(2\rho^2 + Q\right) + \sqrt{\Delta}}{2}\right]^{1/2}; \tag{2.131}$$

$$z_- = -\sqrt{Z_+} = -\left[\frac{-\left(2\rho^2 + Q\right) + \sqrt{\Delta}}{2}\right]^{1/2}. \tag{2.132}$$

Using the values of $8\mu m$ for the diameter, $2\mu m$ for the maximum height of the surface, and $1\mu m$ for the minimum height, we obtain values of $P = -15.12$, $Q = 56.12$ and $R = -14.10$. We can finally plot the red blood cell model:

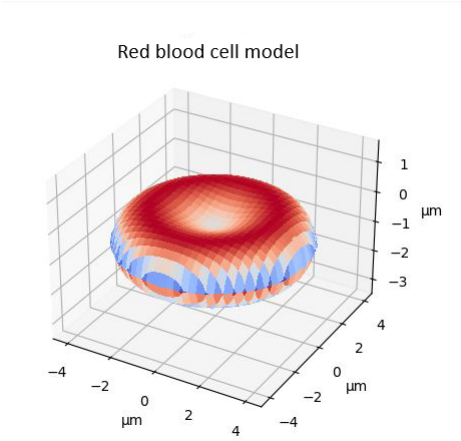

Figure 10 – Surface plotted using equations 2.131 and 2.132.

With the surface area, we can easily define the thickness H and asymmetry ξ for the simulated red blood cell and reverse the process, generating the contrast with the traditional expression 2.66 and the new expression 2.108.

2.3 Diffraction-limited systems

At no point during the propagation of the electric field in the defocused microscope do we take into account that we are in a system limited by diffraction. This not problematic when dealing with experimentally obtained images, but it will be a problem when we calculate the contrast of a simulated phase object, so let us briefly construct the theory of pupil functions and impulse response functions.

Every optical imaging system can be exemplified as shown on figure 11: an object, a "black box" with two openings called pupils, one for input and one for output, which contain all the optical components of the system, and a plane where the image is formed, after the output pupil. The diffraction-limited system is defined as one in which each point on the object plane generates a converging spherical wave, which is collected by the entrance pupil, and in turn, the exit pupil generates a converging spherical wave to the

image plane. Each point on the image plane can be related to the object plane by the same magnification factor in the ideal case.

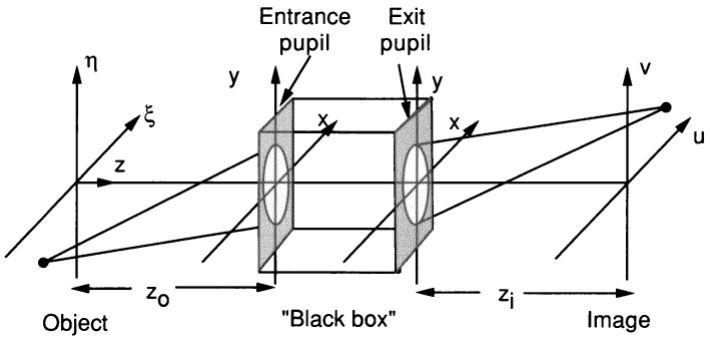

Figure 11 – Diffraction-limited system model. Taken from [22].

We need to study the effects of diffraction on image formation in the case of monochromatic illumination. We can consider that inside the "black box" all effects can be explained by geometric optics, so the entrance and exit pupils must be responsible for the diffraction effects. Since the pupils are images of each other, we can consider that all effects are created by only one of them. The first studies in this regard were conducted by Abbe [23] in 1873, considering only the entrance pupil, and by Rayleigh [24] in 1896, considering the exit pupil. Let us consider the view that diffraction effects are generated solely at the exit pupil. The amplitude of the electric field in the image plane is given by:

$$E_i(u,v) = \iint_{-\infty}^{\infty} h(u,v;\xi,\eta)E_o(\xi,\eta)d\xi d\eta, \tag{2.133}$$

in which E_o is the field in the plane of the object, $h(u,v;\xi,\eta)$ is the amplitude of the field at position (u,v) that was transmitted by the object at position (ξ,η). This function is given by:

$$h(u,v;\xi,\eta) = \frac{A}{\lambda z_i}\iint_{-\infty}^{\infty} P(x,y)e^{\frac{ik}{z_i}[(u-M\xi)+(v-M\eta)]}dxdy, \tag{2.134}$$

where $P(x,y)$ is the pupil function of the exit aperture, located in the plane (x,y), and M is the magnification given by the optical system. To leave equation 2.134 invariant, we use the reduced coordinates $\tilde{\xi} = M\xi$, and $\tilde{\eta} = M\eta$. Making this change:

$$h(u-\tilde{\xi},v-\tilde{\eta}) = \frac{A}{\lambda z_i}\iint_{-\infty}^{\infty} P(x,y)e^{\frac{-ik}{z_i}\left[(u\tilde{\xi})x+(v-\tilde{\eta})y\right]}dxdy. \tag{2.135}$$

We can now define the ideal image E_g, which would be formed in a system not limited by diffraction, given by geometric optics:

$$E_g(\tilde{\xi},\tilde{\eta}) = \frac{1}{|M|}E_o\left(\frac{\tilde{\xi}}{|M|},\frac{\tilde{\eta}}{|M|}\right). \tag{2.136}$$

Using this concept, we obtain a convolution equation for the image:

$$E_i(u,v) = \iint_{\infty}^{\infty} h(u-\tilde{\xi}, v-\tilde{\eta}) E_g(\tilde{\xi},\tilde{\eta}) d\tilde{\xi} d\tilde{\eta}, \tag{2.137}$$

Where:

$$h(u,v) = \frac{A}{\lambda z_i} \iint_{\infty}^{\infty} P(x,y) e^{-\frac{ik}{z_i}(ux+vy)} dxdy. \tag{2.138}$$

We can identify $h(u,v)$ as the Fraunhofer diffraction pattern of the exit pupil of our system. Then, in the general case for monochromatic illumination, the image formed in a diffraction-limited system is the convolution of the ideal image, given by geometric optics, with the Fraunhofer diffraction pattern of the exit pupil.

Finding the exact pupil function of a microscope is extremely complex, requiring techniques such as Fourier Pictography, demonstrated in the article [25], or open-field fluorescence microscopy, as in [26].

As this is a highly complex issue that goes beyond the scope of this work, we will make some approximations.

In the case of the microscope, it is reasonable to assume that all openings through which light passes are circular, and are therefore defined by the function:

$$P(x,y) = \begin{cases} 1, & \text{if } \sqrt{x^2+y^2} \leq R; \\ 0, & \text{if } \sqrt{x^2+y^2} > R, \end{cases} \tag{2.139}$$

where R is the effective pupil opening radius of the system. We can also write it as:

$$P(x,y) = circ\left(\frac{\sqrt{x^2+y^2}}{R}\right). \tag{2.140}$$

The Fraunhofer diffraction pattern of a circular aperture is well known, given by:

$$h(u,v) = \frac{J_1(r)}{r}, \tag{2.141}$$

Where r is the radius in the reciprocal plane, and J_1 is the Bessel function of first order. This function generates the Airy pattern, shown in the figure.12.

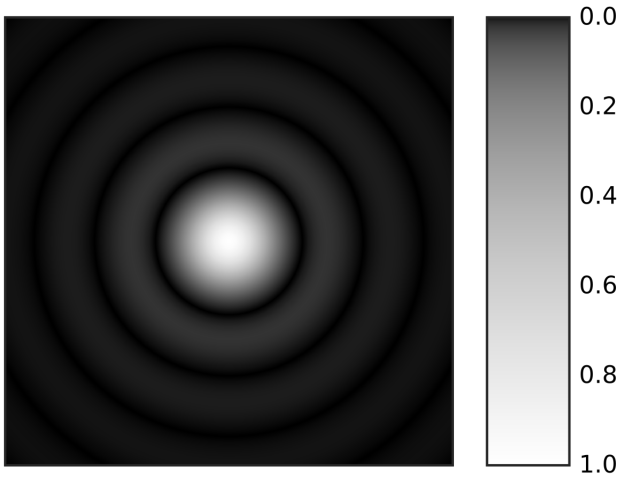

Figure 12 – Airy pattern.

We can approximate the Airy disk by a circle centered on the central maximum, that is:

$$h(f_x, f_y) = circ\left(\frac{\sqrt{f_x^2 + f_y^2}}{R/\lambda.z_i}\right) \tag{2.142}$$

The quantity that now occupies the place of the radius of the function *circ* in 2.142 is called the cutoff frequency f_o and limits the possible spatial frequencies in our system after diffraction. It is given by:

$$f_o = \frac{R}{\lambda z_i}. \tag{2.143}$$

3 Methodology

3.1 Experimental Setup

The experiments were conducted at the Physics of Biological Systems Laboratory in the Physics Department at UFMG. The inverted optical microscope used was a Nikon TI-E model, with a Nikon objective lens of 100x magnification and a numerical aperture of 1.48. Two camera models were used to capture the defocusing microscopy images: an EPIX camera, model SV643M CMOS, with a variable capture rate of up to 26636 frames per second and a pixel size of $0.098\mu m$ on the objective lens used; and a UNIQ camera, model UP1800 CL - 12 bits, with a CCD sensor, a capture rate of 15 frames per second, and a pixel size of $0.064\mu m$ on the 100x objective lens. The equipment is shown in figure 13.

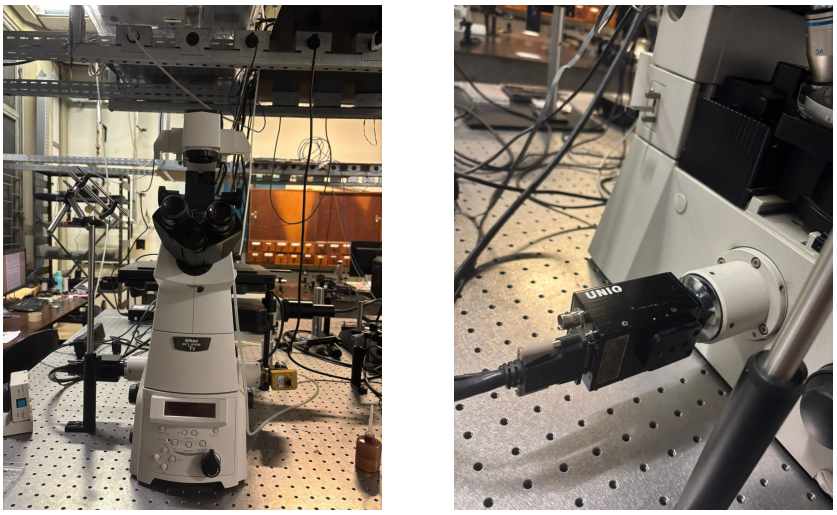

(a) TI-E microscope. (b) UNIQ camera used.

Figure 13 – Microscope and camera used during the experiments.

The microscope has a focus control system called PFS (Perfect Focus System), which is essential for conducting the experiments, since one of the most important variables is the difference between the focal planes of the acquired images. The camera primarily used was a CCD sensor due to the higher image quality, since the low capture rate does not influence the accuracy of the 3D reconstruction. A high-pass red filter was also used to reduce light absorption by red blood cells.

3.1.1 Sample preparation

To prepare the red blood cell samples, three media were prepared: an isotonic buffer solution containing 1 mg of Bovine Serum Albumin (BSA) per mL of Phosphate-buffered Saline (PBS), with an approximate osmolality of 290 mOsm/kg; a hypotonic solution, which is a dilution of the isotonic solution in deionized water in a ratio of 70% solution and 30% water and has an approximate osmolality of 200 mOsm/kg; and a hypertonic solution, which was produced by adding 3.21 mg of NaCl to each mL of the original isotonic solution, resulting in an osmolality of approximately 400 mOsm/kg.

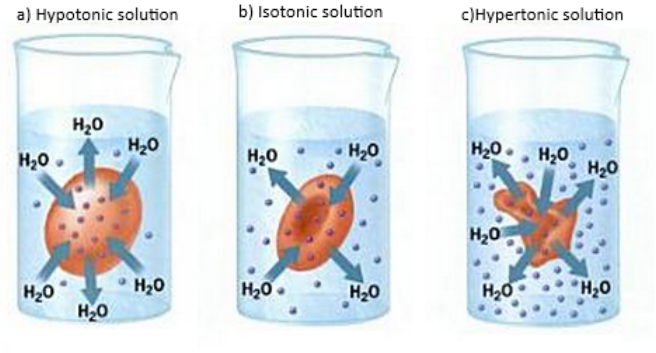

Figure 14 – Change in cell morphology due to the osmolality of the medium. From left to right, we have a red blood cell in hypotonic, isotonic, and hypertonic solutions. adapted from [27].

Sample preparation was the same regardless of the medium chosen: first, 1 mL of solution is placed in an Eppendorf tube. Add 2 μL of blood taken from a student at the time of the experiment to this tube, and homogenize the solution by shaking gently. Place 700 μL of the medium in another Eppendorf tube, along with 200 μL of the blood solution prepared in the first Eppendorf tube. The solution is then homogenized with the help of a micropipette. From the final solution, 600 μL are collected with the micropipette and added to a glass bottom dish, which is then placed on the microscope sample holder. One must wait 15 minutes for the red blood cells to settle before starting the experiment.

During the experiment, two captures are made for each cell: one at minimum contrast, and another with a defocusing of $2\mu m$. In addition to the cell images, a background capture is also made, an area without the presence of cells that is used later to correct camera sensor fluctuations and other constant imperfections in the system. The background correction is performed using the following expression:

$$IC = \frac{I}{Bg} \times \langle Bg \rangle \,, \tag{3.1}$$

in which IC is the corrected image, I is the original image, Bg is the background image, and $\langle Bg \rangle$ is the average value of the background. Image 15 shows the difference between an image before and after correction.

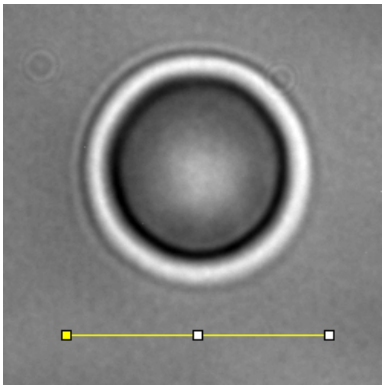

(a) Before correcting *background*.

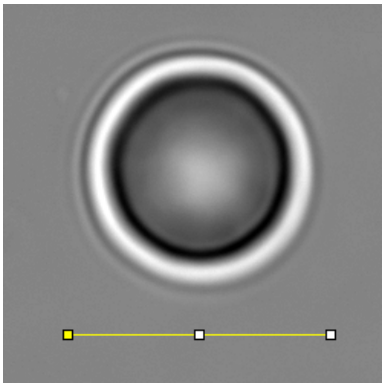

(b) After correcting *background*.

(c) *Background* collected and used for correction.

Figure 15 – Comparison between images before and after correction of the background, together with the background used

A quantitative way to verify the importance of *background* correction is to analyze the variation in gray level along the marked line on the images 15a and 15b as shown in Figure 16.

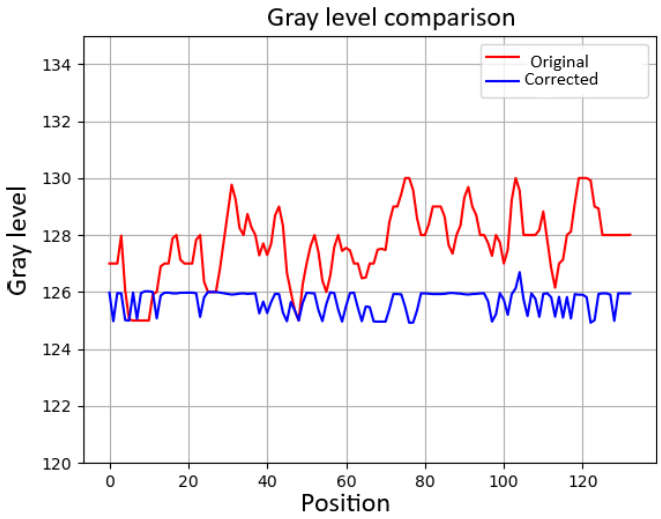

Figure 16 – Gray level comparison.

On average, the experiments last between two and two and a half hours, during which time the red blood cells maintain their stable geometry. After this time, degradation occurs on their surface, with the appearance of roughness. The experiments were carried out at $37°C$ with CO2 control at 5%.

3.2 Computer processing

The images were processed on a laptop with an Intel i7-9750H processor, NVIDIA GeForce GTX 1660 Ti graphics card, and 16 GB of RAM, using the Python programming language.

Once the images with corrected backgrounds were obtained, the OpenCV library was used to import the images, which were then converted to contrast. To find the region in the image where the cell is located, the radial derivative was used on the defocused image contrast, and the coordinates with the maximum derivative were understood as the cell outline, as shown in Figure 17.

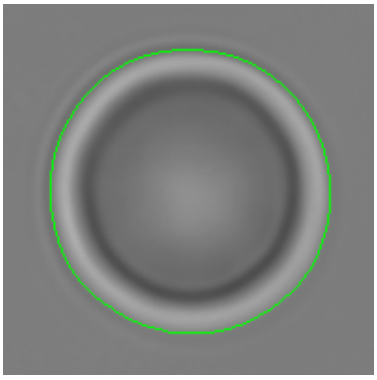

Figure 17 – Example of detected contour.

Due to discontinuities found at the edges of the cell, as we go from cell to background, it is convenient to reduce the contour used to define the region of interest. This is done using a scaling algorithm, and the ratio used may vary from cell to cell, depending on the characteristics of each one. In general, a ratio between 80% and 90% was used. Figure 18 shows an example of the new region explored in the cell.

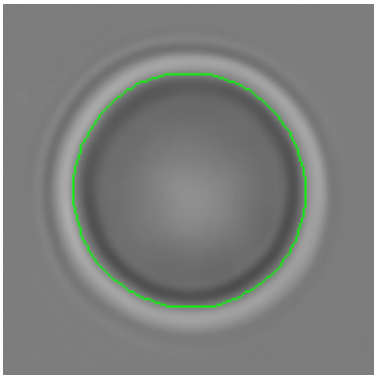

Figure 18 – Example of the new region explored in the figure.

Once the region of interest has been identified, the *numpy* library is used to solve the equations for the thickness $H(\rho)$ and $\xi(\rho)$, which are 2.109 and 2.110 respectively, using the fast Fourier transform algorithm. The approximate radius of the red blood cell is obtained using the Hough transform on the defocused image, an algorithm used to identify circles in images, using the *OpenCV* library.

With the thickness and asymmetry, we then obtain the total 3D reconstruction by writing $h_1 = (\xi + H)/2$ and $h_2 = (\xi - H)/2$. The cell volume is found by integrating the thickness. Mathematically:

$$V = \int H(x, y) dx dy. \tag{3.2}$$

The area of each surface is found using the equation:

$$A_{h_i} = \int \left[1 + \left(\frac{\partial h_i}{\partial x} \right)^2 + \left(\frac{\partial h_i}{\partial y} \right)^2 \right]^{1/2} dx dy \tag{3.3}$$

where $i = 1, 2$. The total surface area of the cell is then the sum of the areas, $A_T = A_{h_1} + A_{h_2}$. With the volume and area, we can calculate the sphericity index χ [28], which compares the profile of the red blood cell to a sphere. It is calculated using the equation:

$$\chi = \frac{\sqrt[3]{36\pi V^2}}{A}. \tag{3.4}$$

The sphericity index has values between 0 and 1, with 1 being a sphere.

4 Results

4.1 Reconstruction of a simulated red blood cell

From the surface shown on image 10, we can use the traditional contrast equation 2.66 to generate the contrast at two different focal planes, shown in the figure 19.

(a) Contrast image at df=0μm. (b) Contrast image at df=2μm.

Figure 19 – Contrasts of the simulated surface of a red blood cell. a) In the position of lowest contrast and b) defocused by 2 μm

We can see that the simulated contrast image shown in image 19b is visually very different from that shown in image 15b, an image with the same defocus. We can draw a horizontal line through the middle of the cell to better observe this difference, as shown in figure 20.

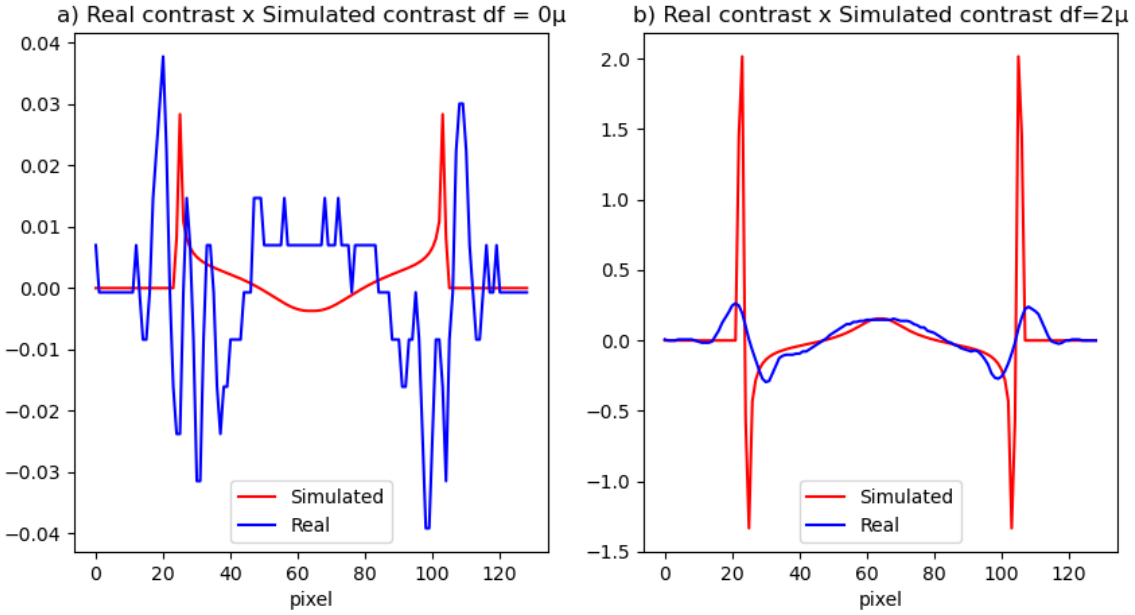

Figure 20 – Comparison between simulated and real contrasts of a red blood cell. In a) we have both contrasts at $df = 0\mu m$, and in b) at $df = 2\mu m$

To approximate our simulated contrast image, we can use the method presented in section 1.3 and convolve the contrast with the microscope's pupil function, which is approximated by an Airy disk. Several radii were tested for the pupil function, three of which are shown on figure 21. The aperture radius used was calculated with equation 2.143.

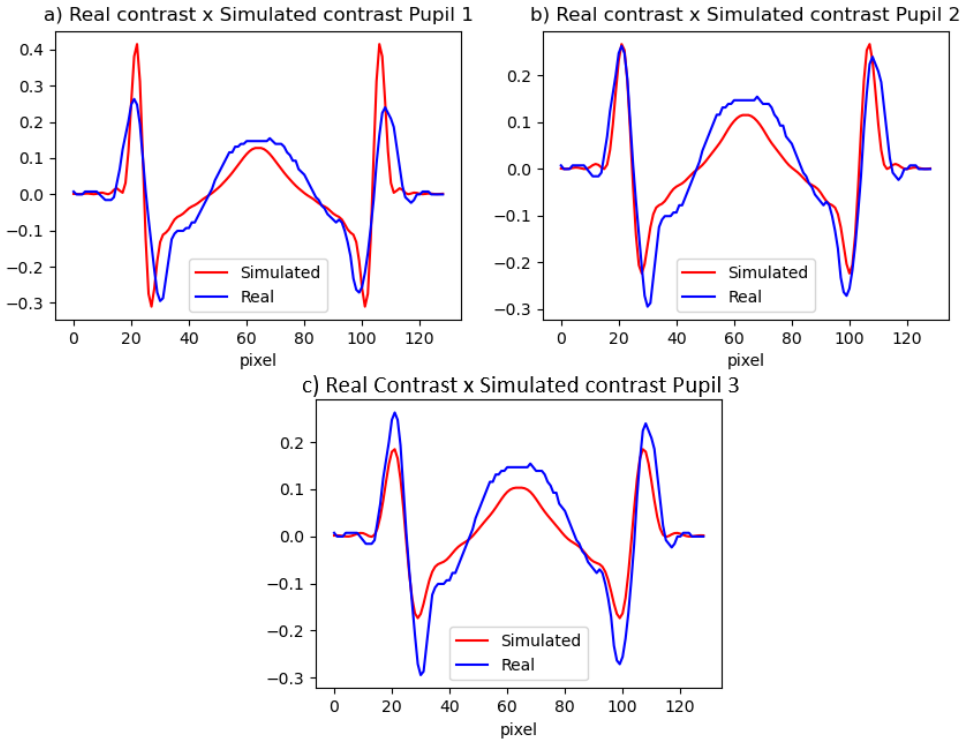

Figure 21 – Comparison between the effect of different pupil functions on the simulated contrast image. In a) we have a pupil with a cutoff frequency $f_0 = 6,85 \times 10^5 m^{-1}$, smaller than that observed in the system; in b) a pupil with a cutoff frequency $f_0 = 6,3 \times 10^5 m^{-1}$, closer to the actual pupil; and in c) a pupil with a cutoff frequency $f_0 = 5,1 \times 10^5 m^{-1}$, larger than that observed.

The pupil chosen as ideal for the work was the one with $f_0 = 6,3 \times 10^5 m^{-1}$. The exit aperture of the objective lens used has a radius of approximately 0.5 cm, resulting in a cutoff frequency $f_0 = 2.5 \times 10^6 m^{-1}$. This tells us that there are other objects in our optical system that limit our resolution, generating greater diffraction and lower resolution. The image of the contrasts at the defocusing of df=0μm and df=2μm is shown on figure 22.

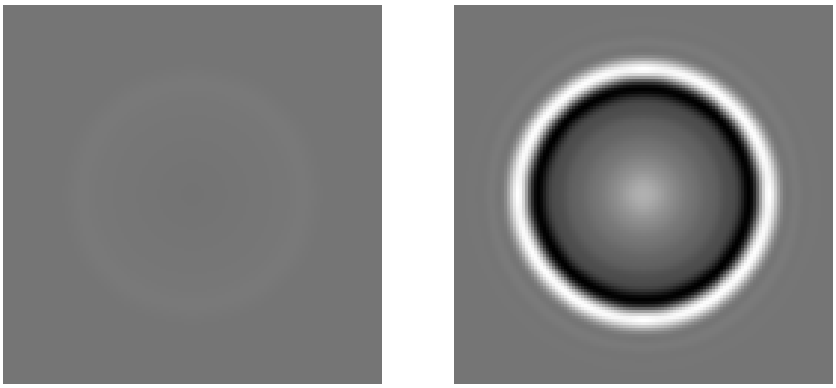

(a) Contrast at df=0μm. (b) Contrast at df=2μm.

Figure 22 – Contrasts of the simulated surface of a red blood cell after convolution.

With those images in hand, we can use them to solve equation 2.69 for thickness

using the computational Fourier transform, and equation 2.71 for asymmetry using the finite element method, discussed in [29].

For thickness, we obtain:

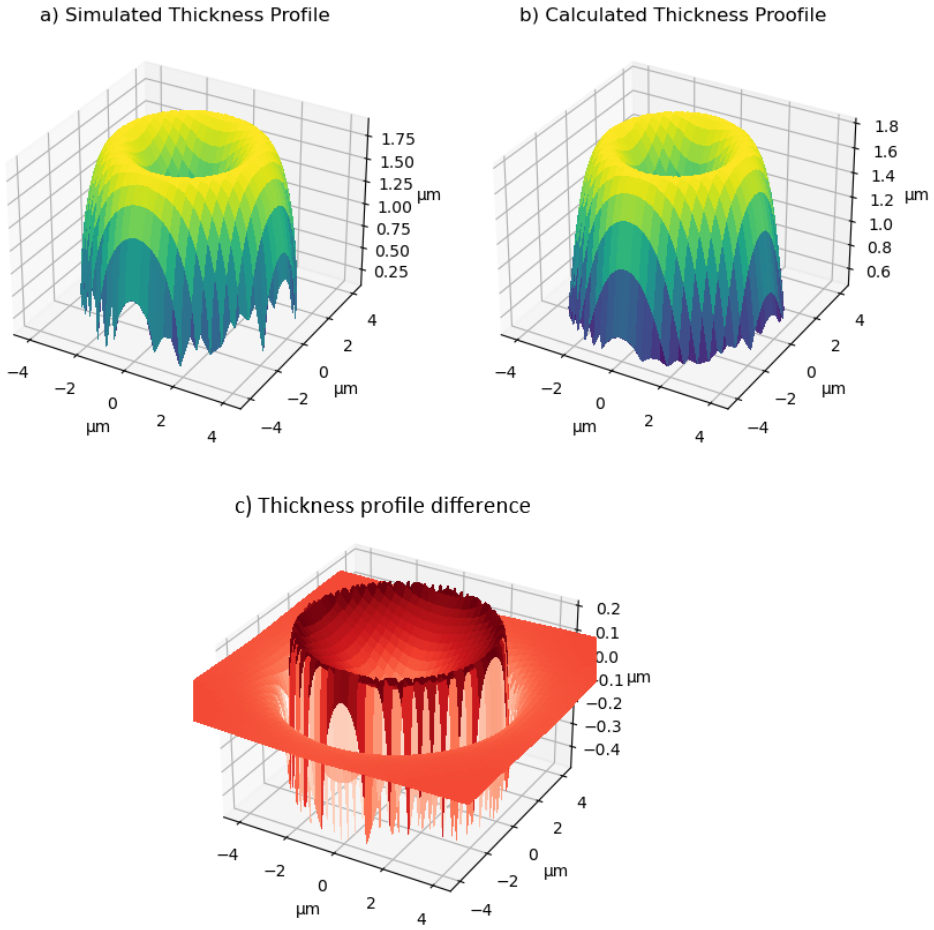

Figure 23 – Comparison of the H thicknesses obtained by solving 2.69 using the images at 22. In a) we have the thickness we expected to obtain again, in b) what we obtain when solving equation 2.69 with the calculated contrasts, and in c) the subtraction of the expected value from the obtained value.

For asymmetry, the solutions obtained are extremely sensitive to contour conditions, as shown on the image below.

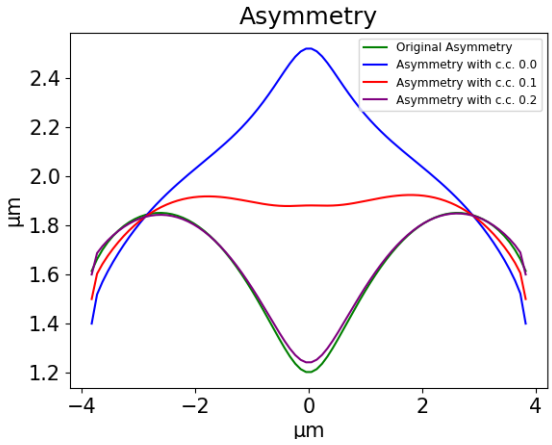

Figure 24 – Difference between asymmetries obtained when solving equation 2.71 with a small variation in the boundary condition.

The high dependence on contour conditions, which cannot be reliably obtained from the image, motivated the search for other ways to solve this problem. This led us to an improved model for the angular spectrum of a phase object and a new expression for contrast.

4.1.0.1 Contrast with refined expression

With the new contrast expression given by equation 2.108, we can again generate the contrast of the phase object with the simulated surface. Again, we convolve the contrast with the chosen pupil function.

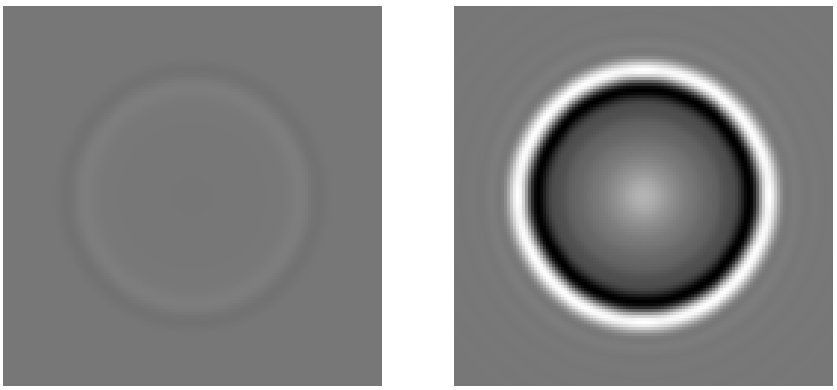

(a) New contrast at df=0μm. (b) New contrast at df=2μm.

Figure 25 – Contrasts of the simulated surface of a red blood cell generated with the expression 2.108.

Compared to the contrast previously used:

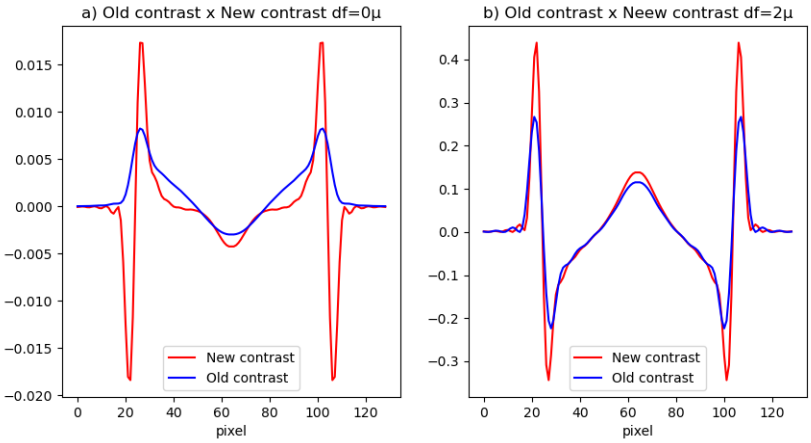

Figure 26 – Comparison between contrasts generated by expressions 2.66 and 2.108. In a) we have the comparison at $df = 0\mu m$, and in b) at $df = 2\mu m$

We then realize that the contrast calculated via the traditional expression, shown in figure 22, and the one calculated via the new expression, figure 25, are extremely similar, so the contrast generated by the new expression is also very similar to the real one, as shown on figure 27.

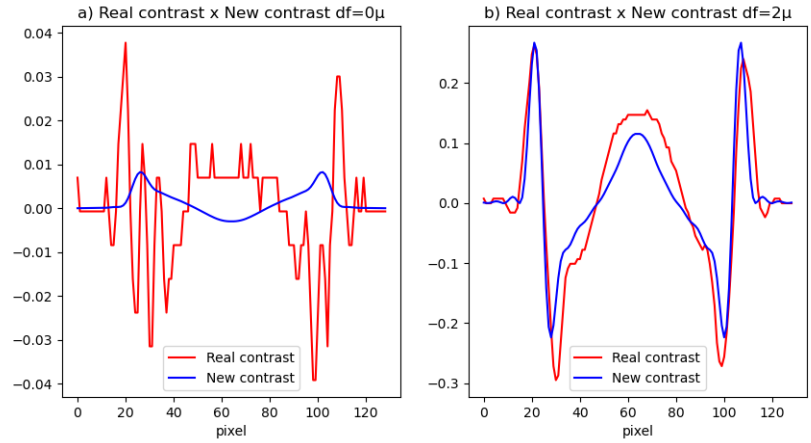

Figure 27 – Comparison between a real red blood cell contrast and the one generated by 2.108. In a) we have the comparison at $df = 0\mu m$, and in b) at $df = 2\mu m$

With the contrasts, we can solve equations 2.109 for thickness and 2.110 for asymmetry, both using the fast Fourier transform in a Python program, which can be found in the appendix of this dissertation. Solving for thickness:

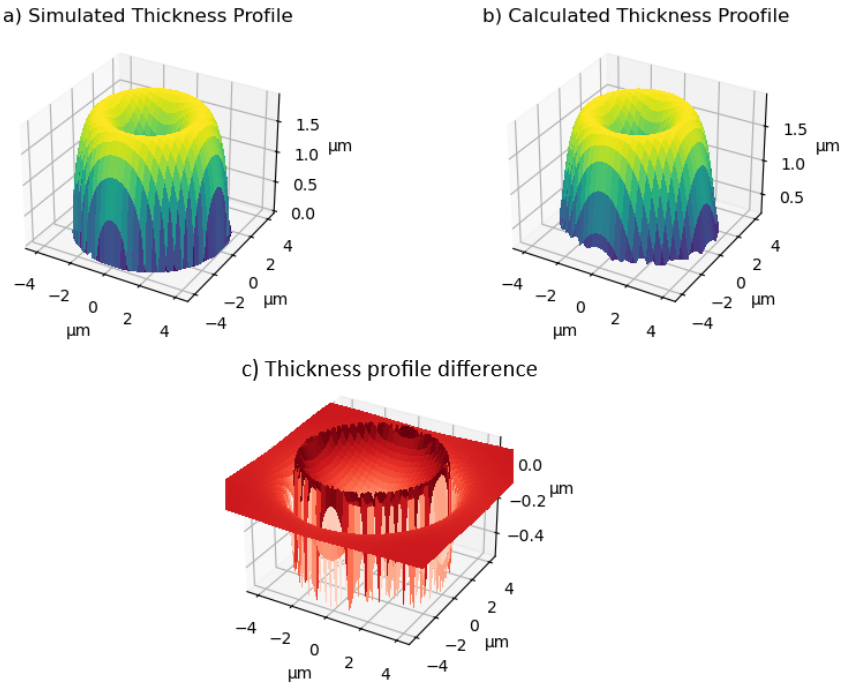

Figure 28 – Comparison of the H thicknesses obtained. In a) we have the thickness we expected to obtain again, in b) what we obtain when solving equation 2.109 with the calculated contrasts, and in c) the subtraction of the expected value from the obtained value.

The thickness was obtained in 0.02s. Looking at the results, we can see on figure 28c) that most of our error is at the edges. This is because the solution obtained by solving the equation for thickness is continuous in its derivative with respect to ρ, while the generated surface goes to zero suddenly at the edges. If we analyze only the center, we observe a difference of approximately 5%, or $0.04\mu m$, between the profiles and the original thickness, demonstrating the effectiveness of the method.

With the thickness, we can calculate the asymmetry from equation 2.110:

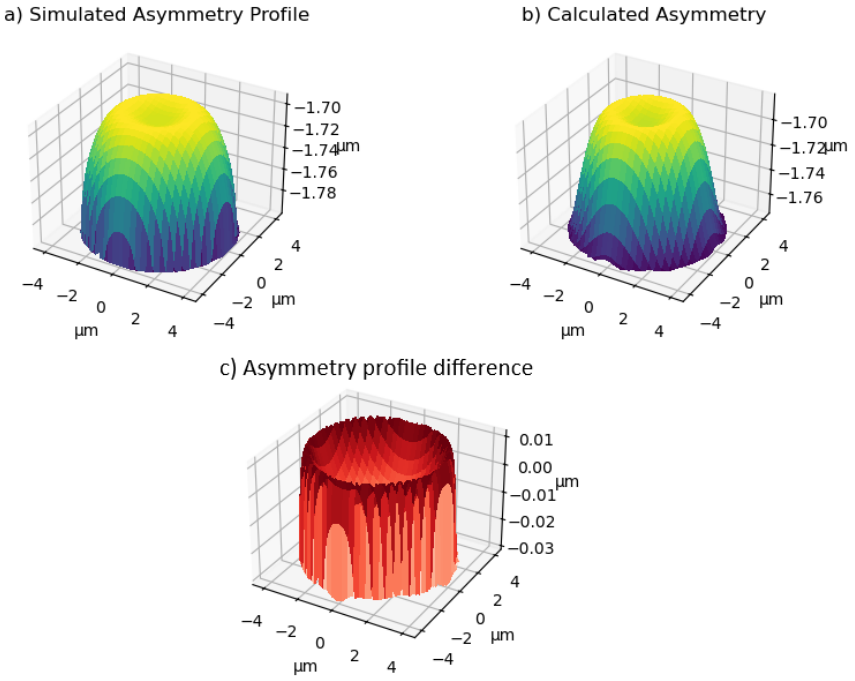

Figure 29 – Comparison of the asymmetries ξ obtained. In a) we have the asymmetry we expected to obtain again, in b) what we obtain when solving equation 2.110 with the calculated contrasts, and in c) the subtraction of the expected value from the obtained value.

Once again, the results were obtained in approximately 0.02s. As in the case of thickness, we can see on Figure 29c) that most of the error obtained is at the edges, again due to the discontinuity of the derivative with respect to ρ in the asymmetry of the generated surface. On the center, an average difference of approximately 5% was observed, this time with a value of $0.08\mu m$.

With the asymmetry and thickness obtained again, we can obtain our surface:

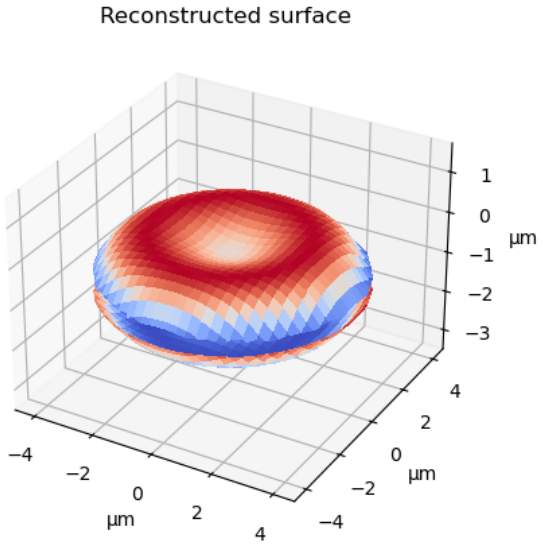

Figure 30 – Surface reconstructed from equations 2.109 and 2.110, with contrasts shown in 25.

The complete program, from surface generation to reconstruction with the generated contrasts, ran in 0.43 seconds.

4.2 Reconstruction of real red blood cells

With the proof of concept carried out on simulated red blood cell surfaces, we can now move on to the reconstruction of real red blood cells. Three media with different osmolalities were used. In the isotonic medium, approximately 30 red blood cells were analyzed, and in the hypotonic and hypertonic media, approximately 25 red blood cells were analyzed in each.

Figure 31 shows the reconstruction of a red blood cell in isotonic medium:

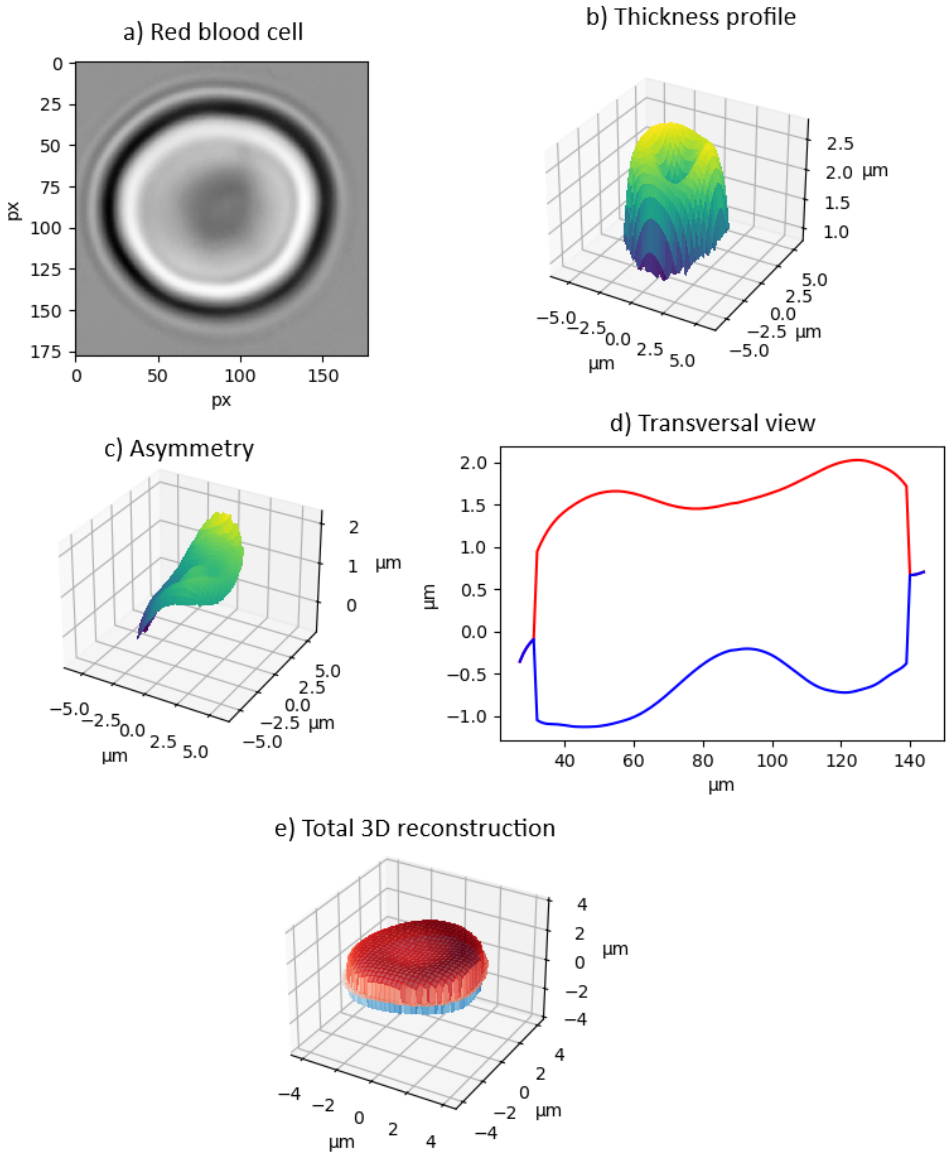

Figure 31 – Three-dimensional reconstruction of a red blood cell in isotonic medium. In a) we have the image of the red blood cell with a defocusing of $2\mu m$, in b) its thickness obtained from equation 2.109, in c) its asymmetry obtained with equation 2.110, in d) a transversal view of the reconstructed red blood cell, and in e) the total three-dimensional reconstruction of the red blood cell. The edges of the surfaces were artificially joined for better visualization. Red blood cell data: $R = 3,7\mu m$, $A = 123,8\mu m^2$, $V = 91,5fL$, $\chi = 0,69$.

On figure 32 below, we show the reconstruction of another red blood cell in isotonic medium, this one with an unusual shape:

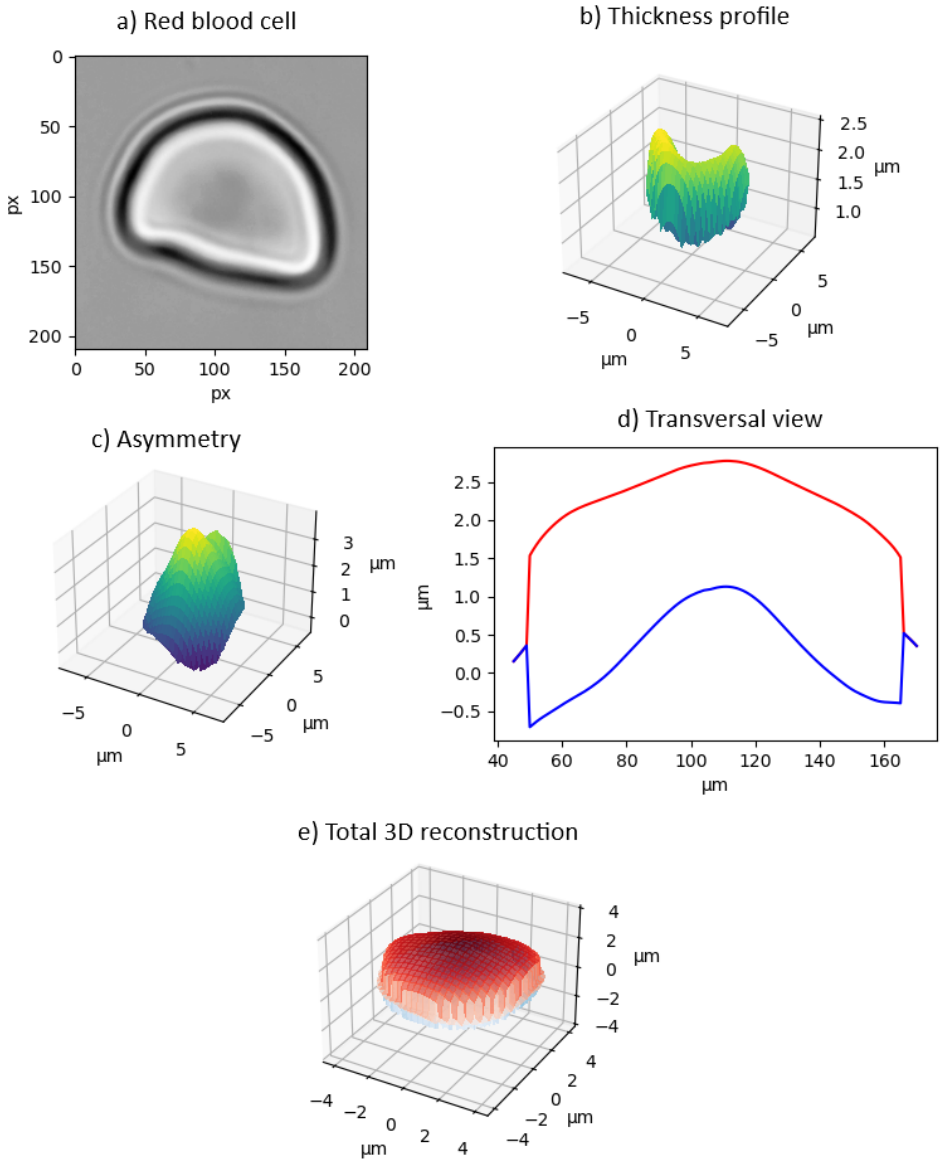

Figure 32 – Three-dimensional reconstruction of an unusually shaped red blood cell in an isotonic medium. In a) we have the image of the red blood cell with a defocusing of $2\mu m$, in b) its thickness obtained from equation 2.109, in c) its asymmetry obtained with equation 2.110, in d) a transversal view of the reconstructed red blood cell, and in e) the total three-dimensional reconstruction of the red blood cell. The edges of the surfaces were artificially joined for better visualization. Red blood cell data: $R = 3,8\mu m$, $A = 131,9\mu m^2$, $V = 84,9fL$, $\chi = 0,71$.

On Figure 33, we have a standard red blood cell in a hypotonic medium:

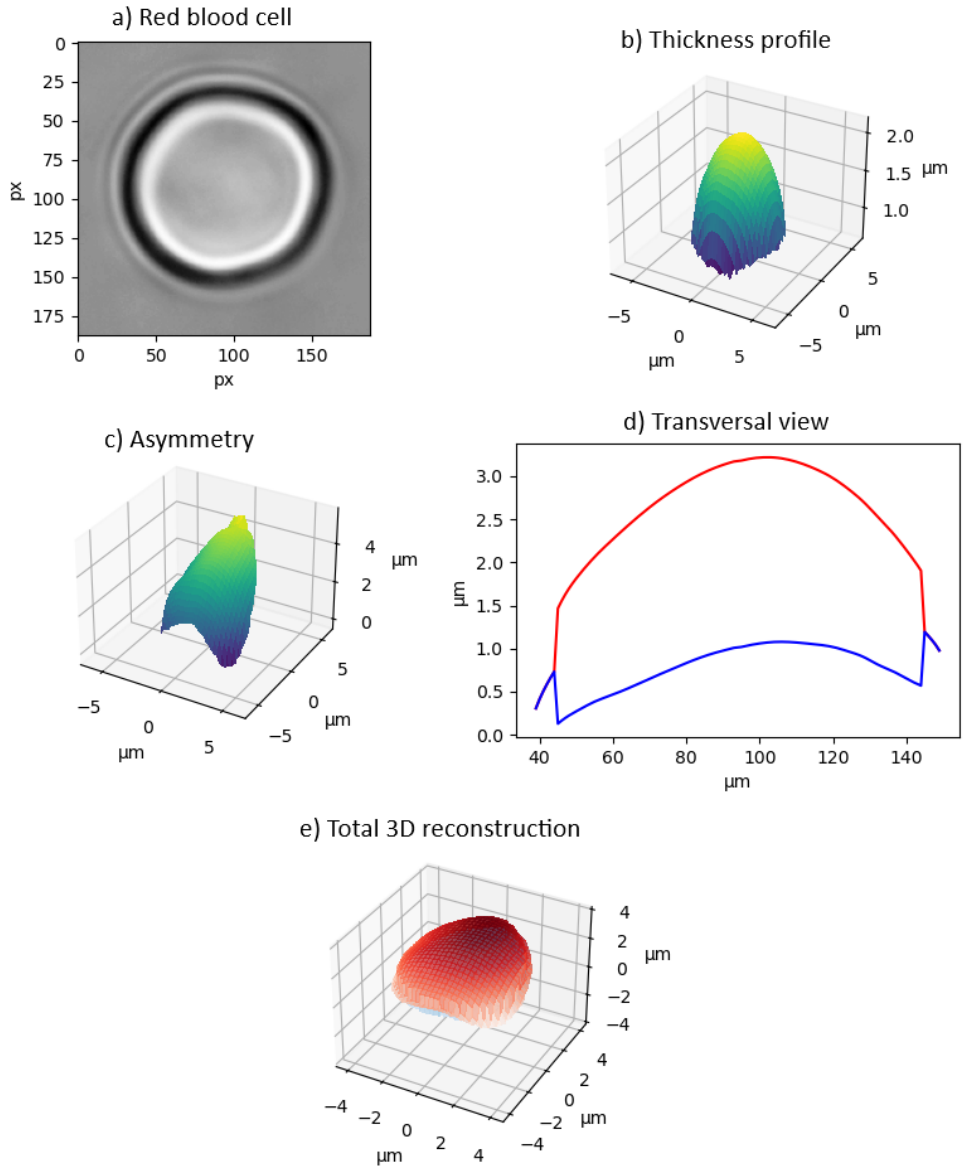

Figure 33 – Three-dimensional reconstruction of a red blood cell in a hypotonic medium. In a) we have the image of the red blood cell with a defocusing of $2\mu m$, in b) its thickness obtained from equation 2.109, in c) its asymmetry obtained with equation 2.110, in d) a transversão view of the reconstructed red blood cell, and in e) the total three-dimensional reconstruction of the red blood cell. $R = 3,5\mu m$, $A = 107,8\mu m^2$, $V = 81,7fL$, $\chi = 0,85$.

And on figure 34, we have another red blood cell in a hypotonic medium:

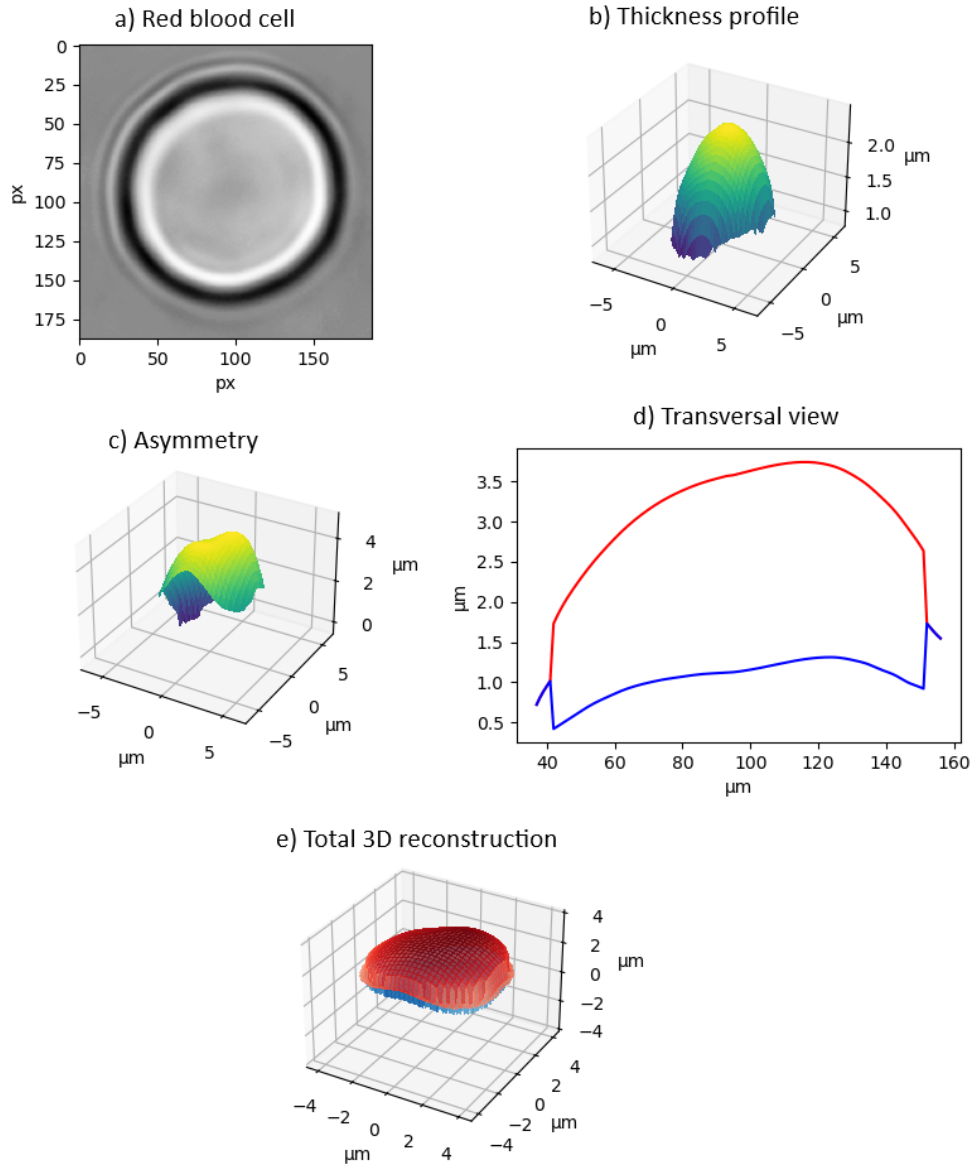

Figure 34 – Three-dimensional reconstruction of a red blood cell in a hypotonic medium. In a) we have the image of the red blood cell with a defocusing of $2\mu m$, in b) its thickness obtained from equation 2.109, in c) its asymmetry obtained with equation 2.110, in d) a transversal view of the reconstructed red blood cell, and in e) the total three-dimensional reconstruction of the red blood cell. The edges of the surfaces were artificially joined for better visualization. Red blood cell data: $R = 3,7\mu m$, $A = 131,4\mu m^2$, $V = 106,2fL$, $\chi = 0,81$.

On figure 35, we have a red blood cell in a hypertonic medium with the expected geometry:

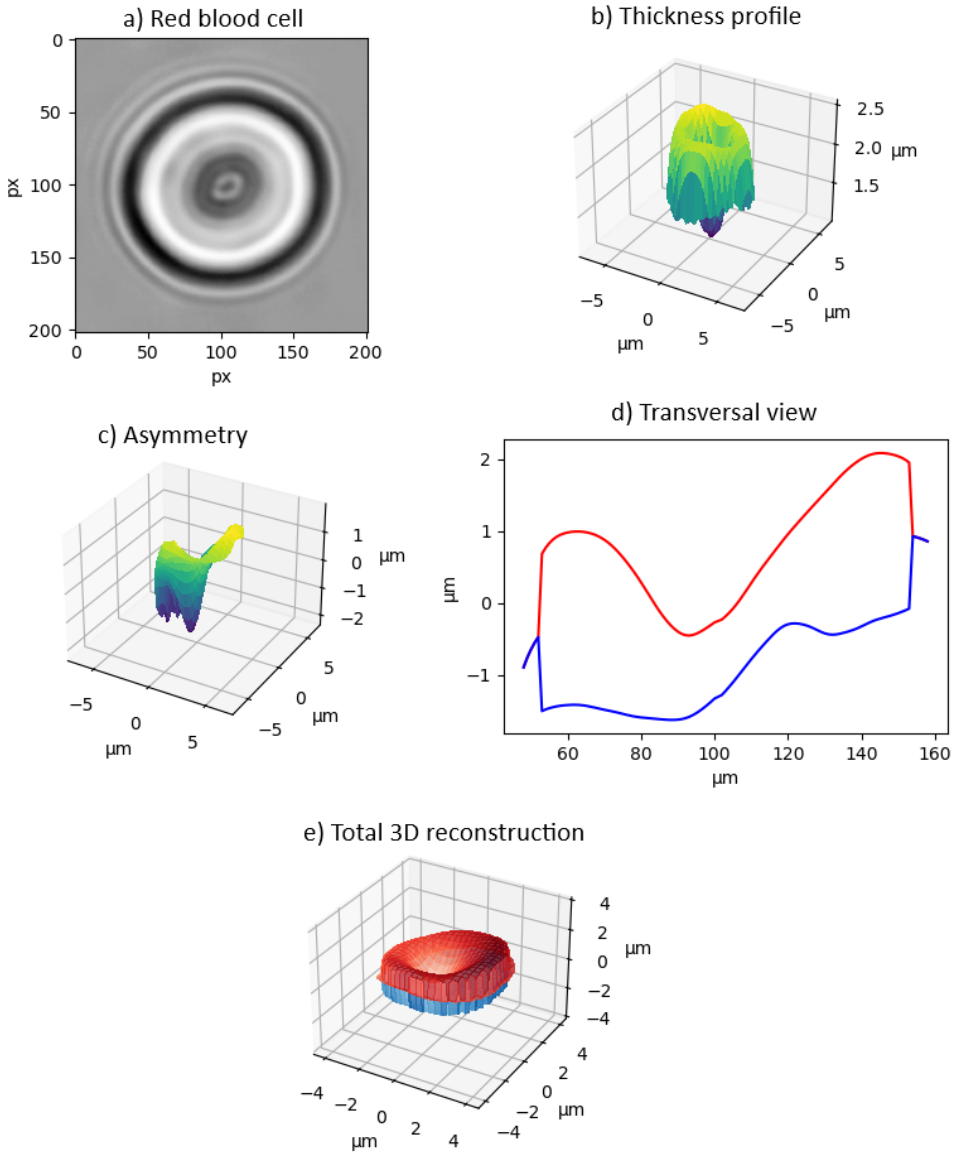

Figure 35 – Three-dimensional reconstruction of a red blood cell in a hypertonic medium. In a) we have the image of the red blood cell with a defocusing of $2\mu m$, in b) its thickness obtained from equation 2.109, in c) its asymmetry obtained with equation 2.110, in d) a transversal view of the reconstructed red blood cell, and in e) the total three-dimensional reconstruction of the red blood cell. The edges of the surfaces were artificially joined for better visualization. Red blood cell data: $R = 2,2\mu m$, $A = 123,3\mu m^2$, $V = 75,2fL$, $\chi = 0,69$.

And on figure 36, another red blood cell in a hypertonic medium:

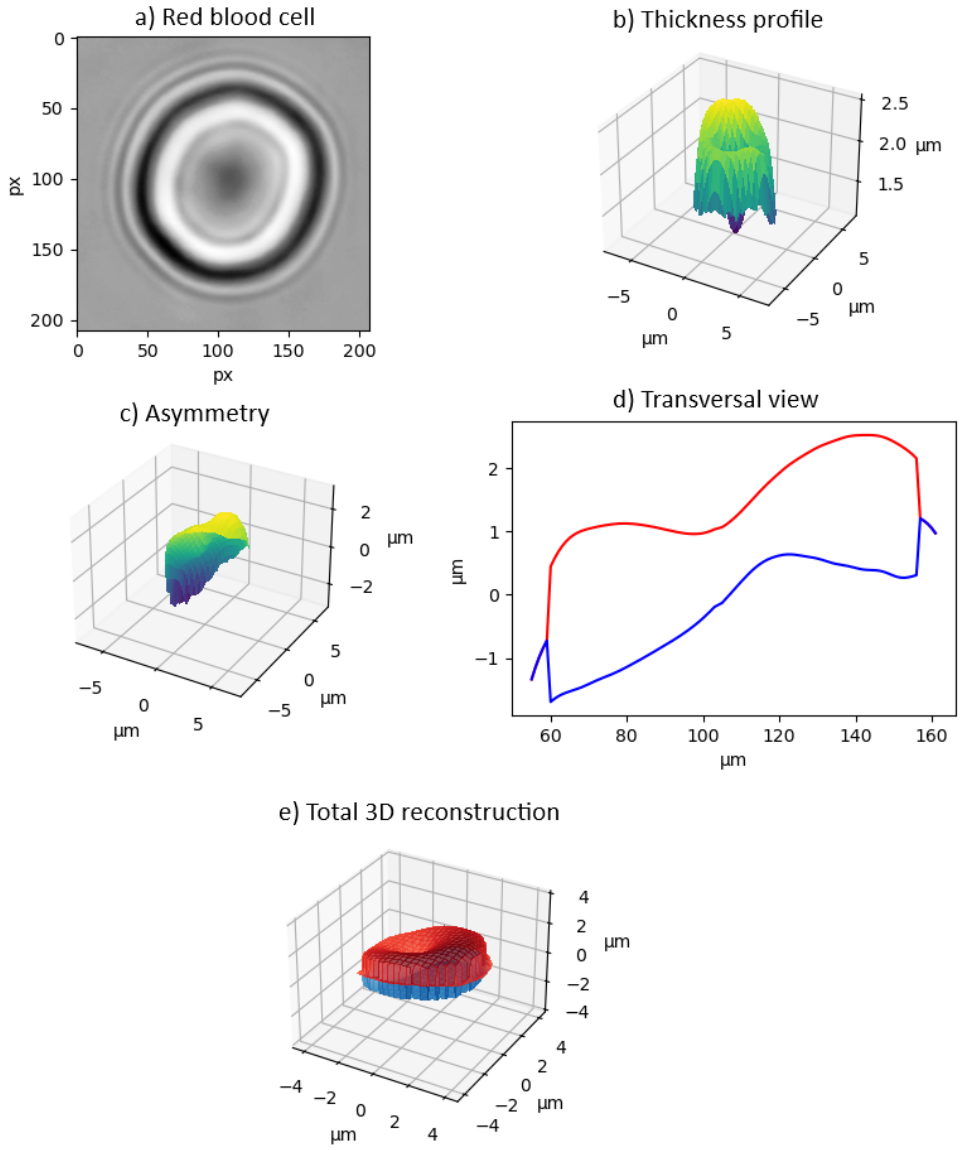

Figure 36 – Three-dimensional reconstruction of a red blood cell in a hypertonic medium. In a) we have the image of the red blood cell with a defocusing of $2\mu m$, in b) its thickness obtained from equation 2.109, in c) its asymmetry obtained with equation 2.110, in d) a transversal view of the reconstructed red blood cell, and in e) the total three-dimensional reconstruction of the red blood cell. $R = 3,5\mu m$, $A = 124,2\mu m^2$, $V = 75,4fL$, $\chi = 0,69$.

We also obtained the average volumes V_M, average total areas A_M, average radii R_M, and average sphericity index χ_M of all red blood cells analyzed. The data were organized in the table below, and errors were calculated based on the standard deviation of the measurement.

Media	$V_M(\mu m^3)$	$A_M(\mu m^2)$	$R_M(\mu m)$	χ_M
Hypotonic	118 ± 26	136 ± 16	$3,6 \pm 0,3$	$0,84 \pm 0,07$
Isotonic	87 ± 14	138 ± 14	$3,7 \pm 0,5$	$0,68 \pm 0,05$
Hypertonic	90 ± 10	152 ± 10	$3,7 \pm 0,3$	$0,64 \pm 0,04$

Analyzing the table, it can be observed that, in general, the results are consistent with those observed in the literature [19], [28] [30]. There was no significant variation between the volume values found in red blood cells in isotonic and hypertonic solutions, contrary to expectations, which may have been due to errors in the preparation of the hypertonic solution, since there was no osmometer available to measure its osmolality. Another possibility is that the solutions were prepared correctly, but in order to observe the osmotic shock more intensely, we should have used a hypertonic solution with even higher osmolality.

5 Conclusion

In this dissertation, we presented the refinement of the model for the angular spectrum of a phase object to be used in defocusing microscopy, as well as its use to create a new expression for the contrast used in the technique. Along with the new expression for contrast, we showed how we can use the surface of an ellipsoid, adjusted so that the surface has a geometry similar to that of a red blood cell, to assist us in testing and validating the computational routine developed for the three-dimensional reconstruction of red blood cells.

With the geometric model, it was possible to visualize the difference between the traditional contrast equation 2.66 and the new one 2.108, and between these and the contrast of a real red blood cell. It was also possible to observe the problems that previously existed with the solution of equation 2.71, which was very sensitive to boundary conditions that cannot be accurately found via experiment.

With the new expression, we were able to perform three-dimensional reconstruction of red blood cells extremely quickly and reliably, taking 0.4 seconds, about 25 times faster than previously presented using the finite element method, as presented in José Maria Caquito's dissertation [29].

With the considerable speed improvement obtained with the new model and computational routine, we can envision that, in the near future, real-time reconstruction will be possible, with the two images in different focal planes being obtained simultaneously in the microscope with the aid of an external module. This also opens up the possibility of analyzing the morphology of red blood cells in dynamic processes, such as when they are stressed by optical tweezers. In addition, the technique may become a means of diagnosing sickle cell anemia, a disease that severely alters the shape and dynamics of the affected red blood cells.

The next steps in the work will be to improve the computational routine in order to enable the reconstruction of red blood cells with images obtained simultaneously under the microscope. The analysis of red blood cells in dynamic situations and the application of the theory to other types of cells, such as macrophages and cardiomyocytes, are also of interest.

Bibliography

[1] F. Zernike. How i discovered phase contrast. *Science*, 121(3141):345–349, 1955. Cited on page 9.

[2] Takahiro Ikeda, Gabriel Popescu, Ramachandra R. Dasari, and Michael S. Feld. Hilbert phase microscopy for investigating fast dynamics in transparent systems. *Opt. Lett.*, 30(10):1165–1167, May 2005. Cited on page 9.

[3] Gabriel Popescu, Takahiro Ikeda, Ramachandra R. Dasari, and Michael S. Feld. Diffraction phase microscopy for quantifying cell structure and dynamics. *Opt. Lett.*, 31(6):775–777, Mar 2006. Cited on page 9.

[4] Pierre Marquet, Benjamin Rappaz, Pierre J. Magistretti, Etienne Cuche, Yves Emery, Tristan Colomb, and Christian Depeursinge. Digital holographic microscopy: a noninvasive contrast imaging technique allowing quantitative visualization of living cells with subwavelength axial accuracy. *Opt. Lett.*, 30(5):468–470, Mar 2005. Cited on page 9.

[5] KyeoReh Lee, Kyoohyun Kim, Jaehwang Jung, JiHan Heo, Sangyeon Cho, Sangyun Lee, Gyuyoung Chang, YoungJu Jo, Hyunjoo Park, and YongKeun Park. Quantitative phase imaging techniques for the study of cell pathophysiology: From principles to applications. *Sensors*, 13(4):4170–4191, 2013. Cited on page 9.

[6] U. Agero, L.G. Mesquita, B.R.A. Neves, R.T. Gazzinelli, and O.N. Mesquita. Defocusing microscopy. *Microscopy Research and Technique*, 65(3):159–165, 2004. Cited 2 times on pages 9 and 73.

[7] Chao Zuo, Jiaji Li, Jiasong Sun, Yao Fan, Jialin Zhang, Linpeng Lu, Runnan Zhang, Bowen Wang, Lei Huang, and Qian Chen. Transport of intensity equation: a tutorial. *Optics and Lasers in Engineering*, 135:106187, 2020. Cited on page 9.

[8] Juan M. Soto, José A. Rodrigo, and Tatiana Alieva. Optical diffraction tomography with fully and partially coherent illumination in high numerical aperture label-free microscopy. *Appl. Opt.*, 57(1):A205–A214, Jan 2018. Cited on page 9.

[9] Juyeon Park, Bijie Bai, DongHun Ryu, Tairan Liu, Chungha Lee, Yi Luo, Mahn Jae Lee, Luzhe Huang, Jeongwon Shin, Yijie Zhang, Dongmin Ryu, Yuzhu Li, Geon Kim, Hyun-seok Min, Aydogan Ozcan, and YongKeun Park. Artificial intelligence-enabled quantitative phase imaging methods for life sciences. *Nature Methods*, 20(11):1645–1660, November 2023. Cited on page 9.

[10] Gabriel Popescu. *Quantitative phase imaging of cells and tissues*. McGraw-Hill biophotonics. McGraw-Hill, New York, 2011. Cited on page 9.

[11] Jonas Gienger, Kathrin Smuda, Ralph Müller, Markus Bär, and Jörg Neukammer. Refractive index of human red blood cells between 290 nm and 1100 nm determined by optical extinction measurements. *Scientific Reports*, 9(1):4623, March 2019. Cited on page 9.

[12] Matti Kinnunen, Antti Kauppila, Artashes Karmenyan, and Risto Myllylä. Effect of the size and shape of a red blood cell on elastic light scattering properties at the single-cell level. *Biomed. Opt. Express*, 2(7):1803–1814, Jul 2011. Cited on page 9.

[13] Paula Magda Roma da Lapa. *Caracterização de parâmetros biomecânicos de hemácias via Microscopia de Desfocalização: Imagem tridimensional total e elasticidade da membrana*. Tese de doutorado, UFMG, 2014. Cited 2 times on pages 17 and 22.

[14] George D. Manolis and Richard P. Shaw. Fundamental solutions to helmholtz's equation for inhomogeneous media by a first-order differential equation system. *Soil Dynamics and Earthquake Engineering*, 16(2):81–94, 1997. Cited on page 23.

[15] Hélène Barucq, Théophile Chaumont-Frelet, and Christian Gout. Stability analysis of heterogeneous Helmholtz problems and finite element solution based on propagation media approximation. *Mathematics of Computation*, 86(307):2129–2157, December 2016. Cited on page 23.

[16] Max Born and Emil Wolf. *Principles of optics: electromagnetic theory of propagation, interference and diffraction of light; 7th ed.* Cambridge University Press, Cambridge, 1999. Cited on page 23.

[17] H. Weyl. Ausbreitung elektromagnetischer wellen über einem ebenen leiter. *Annalen der Physik*, 365(21):481–500, 1919. Cited on page 25.

[18] P. M. S. Roma, L. Siman, F. T. Amaral, U. Agero, and O. N. Mesquita. Total three-dimensional imaging of phase objects using defocusing microscopy: Application to red blood cells. *Applied Physics Letters*, 104(25):251107, 06 2014. Cited on page 32.

[19] Paula Magda S. Roma, Livia Siman, Barbara Hissa, Ubirajara Agero, Erika M. Braga, and Oscar N. Mesquita. Profiling of individual human red blood cells under osmotic stress using defocusing microscopy. *Journal of Biomedical Optics*, 21(9):090505, 2016. Cited 2 times on pages 32 and 60.

[20] P Kuchel. Parametric-Equation Representation of Biconcave Erythrocytes. *Bulletin of Mathematical Biology*, 61(2):209–220, March 1999. Cited 2 times on pages 32 and 33.

[21] Philip W. Kuchel, Charles D. Cox, Daniel Daners, Dmitry Shishmarev, and Petrik Galvosas. Surface model of the human red blood cell simulating changes in membrane curvature under strain. *Scientific Reports*, 11(1):13712, July 2021. Cited on page 32.

[22] Joseph W. Goodman. *Introduction to Fourier optics; Fourth edition*. Macmillan Learning, New York, 2017. Cited on page 37.

[23] Ernst Abbe. Beiträge zur theorie des mikroskops und der mikroskopischen wahrnehmung. *Archiv für mikroskopische Anatomie*, 9:413 – 468, 2009. Cited on page 37.

[24] Rayleigh. XV. On the theory of optical images, with special reference to the microscope. *The London, Edinburgh, and Dublin Philosophical Magazine and Journal of Science*, 42(255):167–195, 1896. Cited on page 37.

[25] Xiaoze Ou, Guoan Zheng, and Changhuei Yang. Embedded pupil function recovery for fourier ptychographic microscopy. *Opt. Express*, 22(5):4960–4972, Mar 2014. Cited on page 38.

[26] B M Hanser, M G L Gustafsson, D A Agard, and J W Sedat. Phase-retrieved pupil functions in wide-field fluorescence microscopy. *J. Microsc.*, 216(Pt 1):32–48, oct 2004. Cited on page 38.

[27] G. Karp. *Biologia celular e molecular*. MANOLE, 2005. Cited on page 41.

[28] P. B. Canham and Alan C. Burton. Distribution of Size and Shape in Populations of Normal Human Red Cells. *Circulation Research*, 22(3):405–422, March 1968. Cited 2 times on pages 44 and 60.

[29] José Maria Caquito Júnior. *Método de elementos finitos aplicado à Microscopia de Desfocalização*. Dissertação de mestrado, UFMG, 2022. Cited 2 times on pages 48 and 61.

[30] C Y Jung. Permeability of bimolecular membranes made from lipid extracts of human red cell ghosts to sugars. *J. Membr. Biol.*, 5(2):200–214, June 1971. Cited on page 60.

Appendix

APPENDIX A – Code for the 3D reconstruction of red blood cells

```
1
2  from mpl_toolkits import mplot3d
3  import cv2
4  import numpy as np
5  import time
6  import matplotlib.pyplot as plt
7  from matplotlib import cm
8  import seaborn
9
10 time_start = time.time()  # begins the time counter
11
12 #%% Reading images with corrected background
13 # The name of the archives needs to be substituted between the ''
14 img_d0 = np.uint8(cv2.imread('26_00-1.tif',2))
15 img_d2 = np.uint8(cv2.imread('26_02-1.tif',2))
16
17 # Contrast calculation
18
19 C0 = (img_d0.astype(float)-np.mean(np.mean(img_d0)))/np.mean(np.mean(img_d0))
20 C2 = (img_d2.astype(float)-np.mean(np.mean(img_d2)))/np.mean(np.mean(img_d2))
21 C=(C2-C0)
22
23 #%% Parameters
24 df_1 =0  # defocus of each image
25 df_2 =2
26 nm = 1.333  # media refractive index
27 nc = 1.391  # red blood cell refractive index
28 nob = 1.51  # objective lens oil refractive index
29 pixelsize = 0.064  # size of the camera's pixel
30 df = df_2 - df_1  # relative defocus between images
31 width,height = img_d2.shape[:2]    # image size parameters
32
33 #%% Finding the cell's contour
34 img_blur = cv2.GaussianBlur(C2,(3,3),0)
35
36 # derivatives so we can find the borders
37 scharrx = cv2.Scharr(img_blur,ddepth=-1, dx=1,dy=0)
38 scharry = cv2.Scharr(img_blur,ddepth = -1,dx=0,dy=1 )
39 scharrXY = np.sqrt(scharrx**2+scharry**2)
40 scharrXY8 = np.uint8(scharrXY)
```

```
41
42  ret,thresh = cv2.threshold(scharrXY8,0,255,cv2.THRESH_BINARY)
43
44  contours, hierarchy = cv2.findContours(image=thresh, mode=cv2.RETR_EXTERNAL,
45                              method=cv2.CHAIN_APPROX_NONE)
46
47  img_copy = C.copy()
48
49  inside = np.zeros_like(C)
50  cv2.drawContours(inside, contours,-1,1,-1 )
51
52  inside = np.uint8(inside)
53
54  cnt,hier = cv2.findContours(inside, mode = cv2.RETR_EXTERNAL,
55                               method = cv2.CHAIN_APPROX_NONE)
56
57  area = []
58
59  for i in cnt:
60      a = cv2.contourArea(i)
61      area.append(a)
62
63  index = np.argmax(area)
64
65  inside2 = np.zeros_like(inside)
66  cv2.drawContours(inside2, cnt, index, 1, -1)
67
68  inside2 = np.uint8(inside2)
69
70  cnt2, hier2 = cv2.findContours(inside2, mode = cv2.RETR_EXTERNAL,
71                              method = cv2.CHAIN_APPROX_NONE)
72
73  #%% If needed, we can alter the size of the contour manually
74
75  inside2 = np.uint8(inside2)
76  cnt2, hier2 = cv2.findContours(inside2, mode = cv2.RETR_EXTERNAL,
77                              method = cv2.CHAIN_APPROX_NONE)
78
79  cntF = cnt2[0]
80  M = cv2.moments(cntF)
81  cx = int(M['m10']/M['m00'])
82  cy = int(M['m01']/M['m00'])
83
84  cnt_norm = cntF - [cx,cy]
85
86  scale = 0.80 # sclae of the new contour relative to the one detected previously
87  cnt_scaled = cnt_norm * scale
88
```

```
cnt_scaled = cnt_scaled + [cx,cy]
cnt_scaled = np.int32(cnt_scaled)

pre_inside = np.zeros_like(C)

cv2.drawContours(pre_inside,cnt_scaled,-1,1,3)

pre_inside = np.uint8(pre_inside)

cntFinal, hierF = cv2.findContours(pre_inside, mode =cv2.RETR_EXTERNAL,
                            method = cv2.CHAIN_APPROX_NONE)

insidef = np.zeros_like(C)

cv2.drawContours(insidef, cntFinal,-1,1,-1)

insidef[insidef==0] = np.nan

#%% Thickness profile

start_H = time.time()

# q^2 parameter construction
freq_x  = np.fft.fftfreq(C.shape[0], pixelsize)
freq_y  = np.fft.fftfreq(C.shape[1], pixelsize)

qxn = 2*np.pi*freq_x
qyn = 2*np.pi*freq_y

mqyn, mqxn = np.meshgrid(qyn,qxn)
Q2n = (mqxn*mqxn) + (mqyn*mqyn)
Q2n[0,0]=1

FdC = np.fft.fft2(C)  # Fourier trtansform of the Delta C

FQ2 = FdC/Q2n

termoH = (2*nob*nm)/(df*(nm**2-nc**2)) # scalar term of the thickness profile expression

H = termoH * np.fft.ifft2(FQ2)  # Thickness profile

H = H.real
H = H + np.abs(np.amin(H))

end_H = time.time()

time_H = end_H - start_H  # time spent on the calculation of H

```

```
137
138 # 3d surface plot
139 H_inside = insidef * H
140 Ny = C.shape[0]
141 Nx = C.shape[1]
142
143 X = np.arange(-Nx/2, Nx/2) * pixelsize
144 Y = np.arange(-Ny/2, Ny/2) * pixelsize
145 X,Y = np.meshgrid(X,Y)
146
147
148 fig = plt.figure()
149 ax = fig.add_subplot(projection='3d')
150 ax.set_xlabel('µm')
151 ax.set_ylabel('µm')
152 ax.set_zlabel('µm')
153
154 ax.set_xlim3d(-4.5, 4.5)
155 ax.set_ylim3d(-4.5, 4.5)
156 # ax.set_zlim3d(-4, 0)
157 plt.title('Thickness profile')
158
159 surf = ax.plot_surface(X, Y, H_inside, cmap=cm.viridis,
160                        linewidth=0, antialiased=False)
161
162 #%% Asymmetry
163
164 start_A = time.time()
165
166 termoA = (4*(nm**2))/((nm**2-nc**2)) # scalar term of the asymmetry expression
167
168 FC0 = np.fft.fft2(C0)  # contrast Fourier transform
169
170 FC0Q2 = FC0/Q2n
171
172 HA = termoA * np.fft.ifft2(FC0Q2)
173
174 HA = HA.real
175
176 A = HA / H # Asymmetry
177
178 end_A = time.time()
179
180 tempo_A = end_A-start_A  # time spent on the calculation of the asymmetry
181
182 HA_inside = HA * insidef
183 A_inside = HA_inside / H_inside
184 # plot 3d da assimetria
```

```
185
186
187 fig = plt.figure()
188 ax = fig.add_subplot(projection='3d')
189 ax.set_xlabel('µm')
190 ax.set_ylabel('µm')
191 ax.set_zlabel('µm')
192
193 ax.set_xlim3d(-4.5, 4.5)
194 ax.set_ylim3d(-4.5, 4.5)
195 # ax.set_zlim3d(-4, 0)
196 plt.title('Assimetria')
197
198 surf = ax.plot_surface(X, Y, A_inside, cmap=cm.viridis,
199                        linewidth=0, antialiased=False)
200
201 # Construction of the srfaces h1 and h2
202
203 h1 = (A_inside + H_inside)/2
204 h2 = (A_inside - H_inside)/2
205
206 #Joining the edges of the surfaces for better visualization
207
208 edge = np.zeros_like(C)
209 cv2.drawContours(edge, cnt_scaled, -1,1,3)
210
211 edge_h1 = edge * h1
212 edge_h2 = edge * h2
213
214 mean = (edge_h1 + edge_h2)/2
215
216 h11 = h1.copy()
217 h22 = h2.copy()
218
219 h11[mean != 0] = mean[mean!=0]
220 h22[mean != 0] = mean[mean!= 0]
221
222 # Surface plot
223
224 fig = plt.figure()
225 ax = fig.add_subplot(projection='3d')
226 ax.set_xlabel('µm')
227 ax.set_ylabel('µm')
228 ax.set_zlabel('µm')
229
230 # ax.set_xlim3d(-4.5, 4.5)
231 # ax.set_ylim3d(-4.5, 4.5)
232 # ax.set_zlim3d(-4, 4)
```

```
233 plt.title('Total 3D reconstruction')
234
235 surf = ax.plot_surface(X, Y, h11, cmap=cm.Reds,
236                         linewidth=0, antialiased=False)
237 surf = ax.plot_surface(X, Y, h22, cmap=cm.Blues,
238                         linewidth=0, antialiased=False)
239
240 #%% Transversal view plot
241
242 mid = int(width/2)
243
244 h11_meio = h22[mid]
245 h22_meio = h11[mid]
246
247 x = np.linspace(0,width, width)
248 x = np.around(x)
249
250 fig = plt.figure()
251 ax = plt.gca()
252 plt.plot(x,h11_meio, color = 'red')
253 plt.plot(x,h22_meio, color ='blue')
254 plt.title('Transversal view')
255 plt.show()
256
257 #%% Radius calculation
258
259 inside_circle =insidef.copy()
260 inside_circle[np.isnan(inside_circle)]=0
261 img = np.uint8(inside_circle * img_d2.copy())
262 circles = cv2.HoughCircles(img,cv2.HOUGH_GRADIENT,1,20,
263                            param1=50,param2=30,minRadius=0,maxRadius=0)
264 circles = np.round(circles[0, :]).astype("int")
265
266 coord_circ = circles[0]
267
268 raio = coord_circ[2] * pixelsize
269
270 #%% Volume calculatiion
271
272 H_calc = H * inside_circle
273 Volume = np.trapz(np.trapz(H_calc,x=None, dx = pixelsize, axis = -1),
274                   x=None, dx = pixelsize, axis = -1)
275
276 #%% Surface Area and sphericity calculation
277
278 h1_calc = h11*inside_circle
279 h2_calc = h22*inside_circle
280
```

```
281 h1_d = np.gradient(h1_calc,pixelsize,pixelsize,axis=[0,1])
282 h1_d2 = np.sqrt(1+h1_d[0]**2+h1_d[1]**2)
283 h1_d2[np.isnan(h1_d2)]=0
284 h1_d2[h1_d2==1.] = 0
285 area_h1 = np.sum(np.sum(h1_d2)) * pixelsize*pixelsize
286
287 h2_d = np.gradient(h2_calc,pixelsize,pixelsize,axis=[0,1])
288 h2_d2 = np.sqrt(1+h2_d[0]**2+h2_d[1]**2)
289 h2_d2[np.isnan(h2_d2)]=0
290 h2_d2[h2_d2==1.]=0
291 area_h2 = np.sum(np.sum(h2_d2)) * pixelsize*pixelsize
292
293 total_area = area_h1+area_h2
294
295 sphericity = (36*np.pi *Volume**2)/total_area
296
297 end_time = time.time()
298
299 total_time= end_time - start_time # total time
300
```

APPENDIX B – *ImageJ* guide for the 3D reconstruction of red blood cells

To begin, we need two images of red blood cells with a relative defocusing of $\Delta z_f = 2\mu m$ and the *plugin* "DivideQ2.class", which was made available by U. Agero in [6]. To install the plugin, we must perform the "Plugins →Install" process and select the file containing the *plugin*.

With the images, the first thing we must do is convert them from grayscale to contrast. Contrast can be given by $C = (I - I_0)/I_0$. To measure I_0, we set up *ImageJ* to "Analyze →Measure" and measure the average gray value for each image. We must now convert the images to *32bit*. We do this using the command "Image →Type →*32bit*". With the images in *32bit*, we calculate the contrasts using "Process →Math →Subtract" and "Process →Math →Divide" with the values previously measured for I_0.

The next step is to calculate the thickness profile of the red blood cell. As previously shown, the thickness can be calculated using equation 2.109. To do this, we must first subtract one image from the other. We do this using "Process →Image Calculator" and choosing the images for subtraction. It is important that the boxes "Create a new window" and "32-bit (float) result" are checked. Mathematically, we have:

$$\Delta C = \frac{(n_m^2 - n_c^2)\Delta z_f}{2n_m n_0}\nabla^2 H. \tag{B.1}$$

We must now calculate the scalar term accompanying the Laplacian of the thickness. n_m is the refractive index of the medium, n_c is the index of the red blood cell, n_0 is that of the oil used in the objective lens, and Δz_f is the relative defocus between the images. The values generally used are $n_m = 1.333$, $n_c = 1.391$, $n_0 = 1.51$ and $\Delta z_f = 2$. Thus, the term is ≈ 0.078. We must then divide ΔC by -0.078. We do this using "Process Math →Divide". To condense the notation, we will do $\frac{(n_m^2 - n_c^2)\Delta z_f}{2n_m n_0} = \alpha$. Now, we have:

$$\frac{\Delta C}{\alpha} = \nabla^2 H. \tag{B.2}$$

Let's solve this differential equation using the Fourier transform method. We will use the Hartley transform $\mathcal{H}$, since we are only interested in the real part of the transform. To select the Hartley transform, we use the option "Process →FFT →FFT Options" and select only the box "Fast Hartley Transform." Running "Process →FFT →FFT" gives us:

$$\frac{1}{\alpha}\mathcal{H}[\Delta C] = q^2\mathcal{H}[H]. \tag{B.3}$$

The Fourier transform inverts the quadrants of the image, so before the next step we must do "Process →FFT →Swap Quadrants". Now, we must use the *plugin* 'DivideQ2'. We do this with the command "Plugins →DivideQ2". Now we have:

$$\mathcal{H}\left[\frac{\Delta C}{\alpha q^2}\right] = \mathcal{H}[H] \tag{B.4}$$

We must now calculate the inverse transform, which for the Hartley transform is equal to the direct transform. We use "Process →FFT →FFT" again, and then we must change the quadrants to their original location by executing "Process →FFT →Swap Quadrants." We are left with:

$$\mathcal{H}\left[\mathcal{H}\left[\frac{\Delta C}{\alpha q^2}\right]\right] = H \tag{B.5}$$

Now we must normalize our image, since Hartley transform normalization has not been performed. To do this, we must divide our image by the window size N twice, since we are performing the operation in two dimensions. Since the "DivideQ2" plugin is in pixels, we must also multiply the image by the camera pixel size p twice to find the value of H in micrometers. Doing this, we finally have:

$$H = \frac{p^2}{\alpha N^2}\mathcal{H}\left[\mathcal{H}\left[\frac{\Delta C}{\alpha q^2}\right]\right] \tag{B.6}$$

Finally, we have found the thickness profile of our red blood cell. Now, let's find the asymmetry, given by equation 2.110.

According to the theory of defocusing microscopy, the contrast is given by:

$$C = \frac{|n_m^2 - n_c^2|}{4n_m^2}\nabla^2\left[H\xi + \frac{2n_m}{n_0}z_f H\right] \tag{B.7}$$

Now choose one of the images used previously, preferably the one with the greatest defocusing. Divide the image by the term $\frac{|n_m^2-n_c^2|}{4n_m^2} = \beta$, using the command "Process →Math →Divide". Using the same values from the thickness calculation, we have $\beta \approx 0.022$. We are left with:

$$\frac{C}{\beta} = \nabla^2\left[H\xi + \frac{2n_m}{n_0}z_f H\right] \tag{B.8}$$

Again, let's calculate the Hartley transform by doing "Process →FFT →FFT", and let's invert the quadrants using "Process →FFt →Swap Quadrants". At the moment we have:

$$\frac{1}{\beta}\mathcal{H}[C] = q^2\mathcal{H}\left[\left(H\xi + \frac{2n_m}{n_0}z_f H\right)\right] \tag{B.9}$$

Now we use the *plugin* "DivideQ2" by going to "Plugins→DivideQ2". Then we have:

$$\frac{1}{\beta q^2}\mathcal{H}[C] = \mathcal{H}\left[\left(H\xi + \frac{2n_m}{n_0}z_f H\right)\right] \tag{B.10}$$

We can now perform the Hartley transform again using "Process →FFT →FFT", followed by returning the quadrants to their original state using "Process →FFT →Swap Quadrants". We are left with:

$$\mathcal{H}\left[\frac{1}{\beta q^2}\mathcal{H}[C]\right] = \left(H\xi + \frac{2n_m}{n_0}z_f H\right) \tag{B.11}$$

We must now perform the same normalization as before, dividing twice by the window size and multiplying twice by the pixel size:

$$\frac{p^2}{N^2}\mathcal{H}\left[\frac{1}{\beta q^2}\mathcal{H}[C]\right] = \left(H\xi + \frac{2n_m}{n_0}z_f H\right) \tag{B.12}$$

Finally, we divide the image by the one obtained previously for the thickness profile, running "Process →Image Calculator" and selecting the two images. We are left with:

$$\xi + \frac{2n_m}{n_0}z_f = \frac{p^2}{HN^2}\mathcal{H}\left[\frac{1}{\beta q^2}\mathcal{F}[C]\right] \tag{B.13}$$

Finally we have obtained both the thickness profile and asymmetry. We can calculate each membrane by doing "Process →Image Calulator" and adding or subtracting H and ξ. After that, we just need to divide each image by two using "Process →Math →Divide", and we have the images for both membranes. To display both membranes individually, we need to execute "Analyse →Surface plot".